geologicaacta

Citation: Mutlu, S., 2025. Tectonic Geomorphology of the Şemdinli Yüksekova Fault Zone (SYFZ) and Başkale Fault Zone (BFZ) (SE Turkey): Evidence from Morphometric Analysis and Neotectonic Structures. Geologica Acta, 23.23, 1-pgs. DOI: 10.1344/GeologicaActa2025.23.23

Online ISSN: 1696-5728

Tectonic Geomorphology of the Şemdinli Yüksekova Fault Zone (SYFZ) and Başkale Fault Zone (BFZ) (SE Turkey): Evidence from Morphometric Analysis and Neotectonic Structures

Sacit Mutlu

Van Yuzuncu Yıl University, Disaster Management and Earthquake Application and Research Center
6508, Van-Turkey. E-mail: sacitmutlu@yyu.edu.tr

ABSTRACT

The collision between the Arabian and Eurasian plates resulted in the uplift of The East Anatolian Province of Shortening (EAPS). Within the EAPS, the faulting mechanism is characterized by right- and left-lateral strike-slip faults, thrust faults, and a relatively limited occurrence of normal faults. When examined on a regional tectonic scale, about 70% of the deformation of the EAPS is controlled by strike-slip faults. However, the proportion of right- and left-lateral strike-slip faults contributing to this deformation remains unknown and is poorly understood. Two adjacent fault zones located at the southeastern margin of EAPS were selected to investigate the deformation associated with right- and left-lateral strike-slip mechanisms using morphometric analysis along with field observations. These fault zones are the Şemdinli Yüksekova Fault Zone (ŞYFZ), which exhibits right lateral deformation and is defined as a seismic gap, and the Başkale Fault Zone (BFZ), which has a left lateral deformation and that caused a destructive earthquake in (23/02/2020, Mw: 5.9). To elucidate the relative degree of active tectonics of both fault zones, morphometric analysesis were applied alongside field surveys. An adaptation of the relative active tectonic Index (Iat) was computed for Başkale and Yüksekova-Şemdinli sub-basins in the region. The results supported by field observations indicate that the drainage basins are largely controlled by fault activity and exhibit a youthful topographic character. Moreover, quantitative data derived from the Index of Active Tectonics (IAT) reveal that the SYFZ demonstrates very high tectonic activity, while the BFZ displays moderate levels of active tectonic deformation. These numerical findings, which indicate ongoing deformation, are further corroborated by field observations that clearly reflect the surface expressions of tectonic activity.

KEYWORDS | **Başkale Fault Zone. Deformation sharing. Morphometric Index. Tectonic geomorphology. Şemdinli-Yüksekova Fault Zone.**

INTRODUCTION

Anatolia is located in the Eastern Mediterranean region of the Alpine-Himalayan orogenic system, formed between the African, Arabian, and Eurasian plates (Fig. 1A). The main tectonic structures in Anatolia formed by collision of (the East Anatolian Province of Shortening (EAPS), North Anatolian Fault, East Anatolian Fault, etc.) was formed by the collision of the African/Arabian and Indian plates with the Eurasian plate to the north (Şengör, 1979; Şengör and Yazıcı, 2020; Şengör and Yılmaz, 1981). As a consequence, EAPS, which forms the Turkey-Iran Plateau (TIP) (Fig. 1B), has driven a westward escape of the Anatolian Block along the North Anatolian Fault Zone and the Eastern Anatolian Fault Zone, contributing to the expansion of the Aegean Sea in western Turkey (Dewey *et al.*, 1986; McKenzie, 1970, 1972; Şengör and Yılmaz, 1981). EAPS is primarily affected by a north-

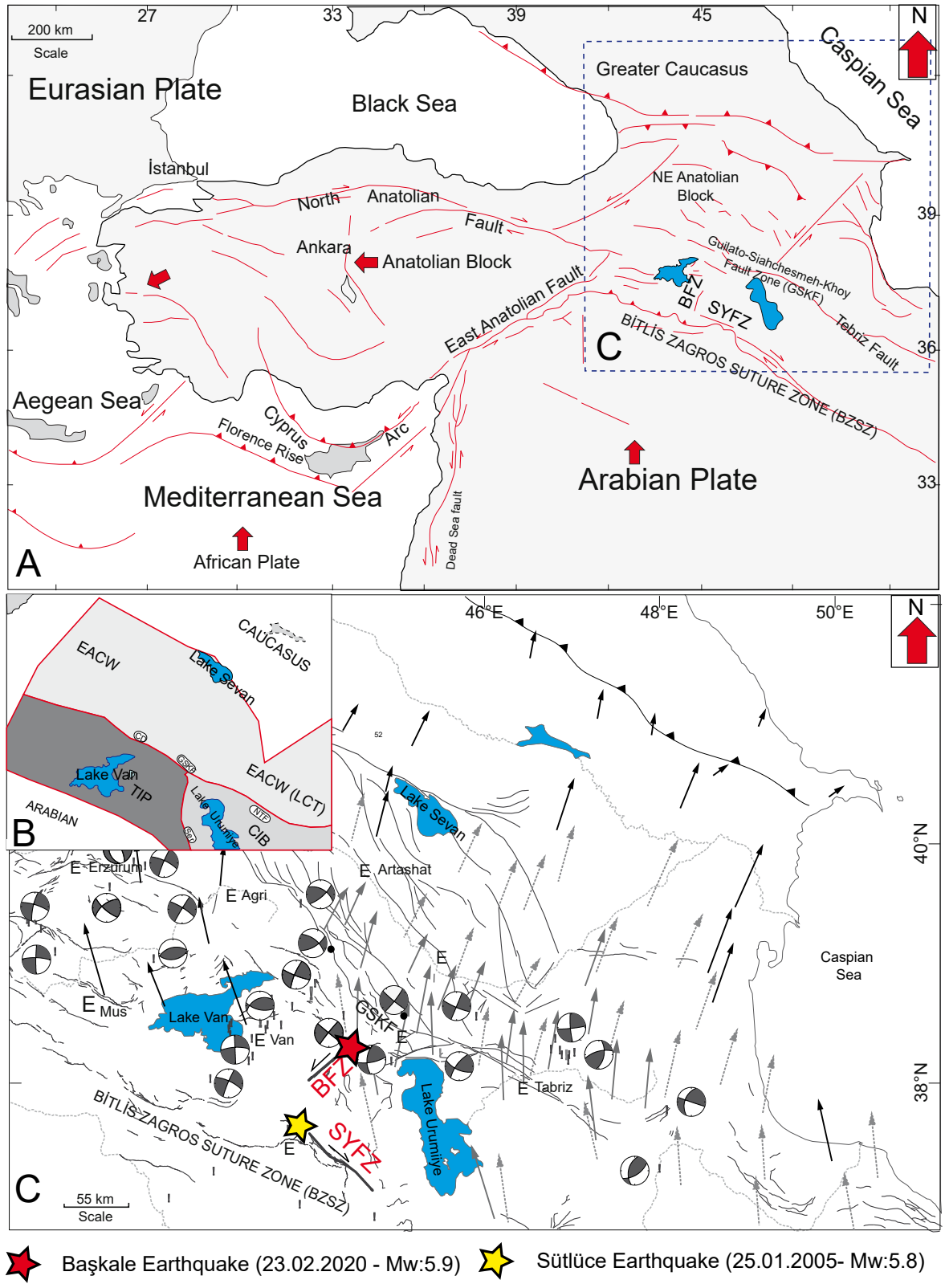

FIGURE 1. A) Neotectonic map of Turkey (Emre *et al.*, 2013; Hessami *et al.*, 2003; Karakhanian *et al.*, 2004; Philip *et al.*, 2001), BFZ: Başkale Fault Zone, ŞYFZ: Şemdinli Yüksekova Fault Zone, BZSZ: Bitlis Zagros Suture Zone. B) Tectonic blocks of the East Anatolian province of shortening, EACW= Eastern Anatolian Collision Wedge (Djamour *et al.*, 2011; Şengör and Yazıcı, 2020), CIB: Central Iranian Block, TIP: Turkish-Iranian Plateau, LCT: Lesser Caucasus-Talesh Block. C) Global Navigation Satellite System (GNSS) velocity field of the East Anatolian province of shortening (Djamour *et al.*, 2003, 2011).

south compressional faulting mechanism resulting from the collision and subsequent post-collisional convergence (Şengör and Yazıcı, 2020). The Turkey-Iran Plateau, has an average elevation of 2 km and represents a significant and prominent region within the Arab-Eurasian plate collision zone. EAPS lies to the north of this plateau, the Arabian Block to the south —bounded by the Bitlis-Zagros Suture Zone (BZSZ)— and the Central Iranian Block to the East (Fig. 1C). Due to north-south compression within EAPS, the region has developed NW-SE and NE-SW trending strike-slip faults, e-E-W oriented thrust faults and bends, N-S oriented normal faults, and extensional slope fracture that define the locations of key volcanic centers. Although it is well established that the ongoing deformation in the region is controlled by numerous active tectonic structures, the deformation rates, slip rates, and kinematic characteristics of the faults within the EAPS and the Turkey-Iran Plateau remain a subject of ongoing debate. (Sançar, 2021; Toksöz and Reilinger, 1992). Analysis of the faults within the EAPS reveals that approximately 70% of the deformation is attributed to strike-slip faults (Ambraseys and Finkel, 1995; Ergin *et al.*, 1967; Karakhanian *et al.*, 2004; Koçyiğit *et al.*, 2001; Sağlam Selçuk, 2016; Soysal *et al.*, 1981; Tan *et al.*, 2008). However, only a limited number of studies have been undertaken to investigate contribution of right-lateral and left-lateral strike-slip faults in this deformation. Another noteworthy aspect is that while numerous right-lateral strike-slip faults are present within EAPS, left-lateral strike-slip faults are relatively scarce. The Başkale Fault Zone (BFZ) is located in close proximity to the Şemdinli–Yüksekova Fault Zone (ŞYFZ) and represents the longest left-lateral strike-slip fault zone within EAPS. According to rigid block models based on GPS data, the Hakkari block—which encompasses both the Başkale and Yüksekova basins—moves in a counterclockwise direction (Reilinger *et al.*, 2006; Djamour *et al.*, 2011). As a result of this motion, higher uplift rates are observed in the western part of the Başkale Basin, while these rates decrease towards the east. It has been reported that uplift rates increase from east to west across the Hakkari block (Sağlam Selçuk and Düzgün, 2017). In the case of the Yüksekova Basin, uplift rate variations occur fourfold in the west and threefold in the east (Sançar, 2018). In summary, the basins controlled by both the BFZ and the ŞYFZ show greater deformation and higher uplift rates in the west (Sağlam Selçuk and Düzgün, 2017; Sançar, 2018). However, the tectonic relationship between the BFZ and ŞYFZ remains unclear. Accordingly, this study aims to determine the IAT of these two fault zones—characterized by different strike-slip directions and clearly traceable in the morphology—through morphometric analysis, as well as to map their morphotectonic features and measure displacements using field observations and aerial/satellite imagery. These data are then used to compare the deformation associated with each fault zone and to infer regional tectonic deformation patterns.

GEOLOGICAL SETTING AND SEISMICITY

Located at the southeastern end of the Turkish-Iranian tectonic block (Fig. 1B), as defined by Global Navigation Satellite System (GNSS) modeling (Fig. 1C) North of the BZSZ (Djamour *et al.*, 2011; Reilinger *et al.*, 2006), the Şemdinli-Yüksekova Fault Zone (ŞYFZ) and the Başkale Fault Zone (BFZ) are situated between active fault zones exhibiting two different lateral directions (Akkaya, 2015; Demirtaş and Yılmaz, 1996; Emre *et al.*, 2005; Koçyiğit, 2005; Sağlam Selçuk and Düzgün, 2017; Sançar, 2018; Şaroğlu *et al.*, 1992; Seyitoğlu *et al.*, 2018).

The ŞYFZ is located along the northeastern extension of the in Turkey (Fig. 2A), and functions as a strike-slip and vertical component transfer fault between the BZSZ and the Zagros Fold–Thrust Belt in Iran (Akkaya, 2015; Hull *et al.*, 2002; Sançar, 2018). The ŞYFZ is an active, right-lateral strike-slip fault zone trending in a NW–SE direction with an approximate length of 110km (Emre *et al.*, 2005; Saroglu, 1985; Saroglu *et al.*, 1987). At the same time, the kinematics and fault orientation of the ŞYFZ are responsible for the formation of the Yüksekova Basin, which represents a pull-apart basin (Fig. 2B). The most prominent morphotectonic structure of the ŞYFZ is the Yüksekova Basin, which extends in a NW-SE direction, with a length of 38km and a maximum width of 10km. In contrast to the Yüksekova Basin, the Başkale Basin, which exhibits a narrower basin characteristic, extends in a NE-SW direction and is approximately 4 Km wide and 82km long (Fig. 2B). The flow direction of the Başkale Basin is toward the south, whereas the flow direction of the Yüksekova Basin is toward the nortwest (Fig. 5). The flow direction of both basins is towards the Zap River. Beyond the Turkish border, this river extends southeastward into Iran, aligning with the Piranshahr fault zone (Fig. 2A), which is part of the main active fault system in the region (Berberian, 1981; Hessami *et al.*, 2003; Saroglu *et al.*, 1987; Tchalenko and Braud, 1974).

Given that the ŞYFZ (Fig. 2B) has no historical earthquake records and that the seismic activity during the instrumental period has been characterized by small-magnitude events, this fault zone is classified as a seismic gap (Demirtaş and Yılmaz, 1996). The BFZ is located between the Guilato Siahcheshmeh–Khoy Fault Zone and the ŞYFZ (Fig. 2A). The BFZ is a left-lateral strike-slip fault zone, approximately 82 km in length, exhibiting a normal component in the K10-40D direction. Although the width of the basin is less than that of the ŞYFZ, it provides a basin area with a width of around 4km. The BFZ, which has been the subject of a limited number of studies (Emre *et al.*, 2005, 2012; Koçyiğit, 2005; Sağlam Selçuk and Düzgün, 2017), was first mapped by Koçyiğit (2005) following the Sütlüce Earthquake (25.01.2005, Mw= 5.8)

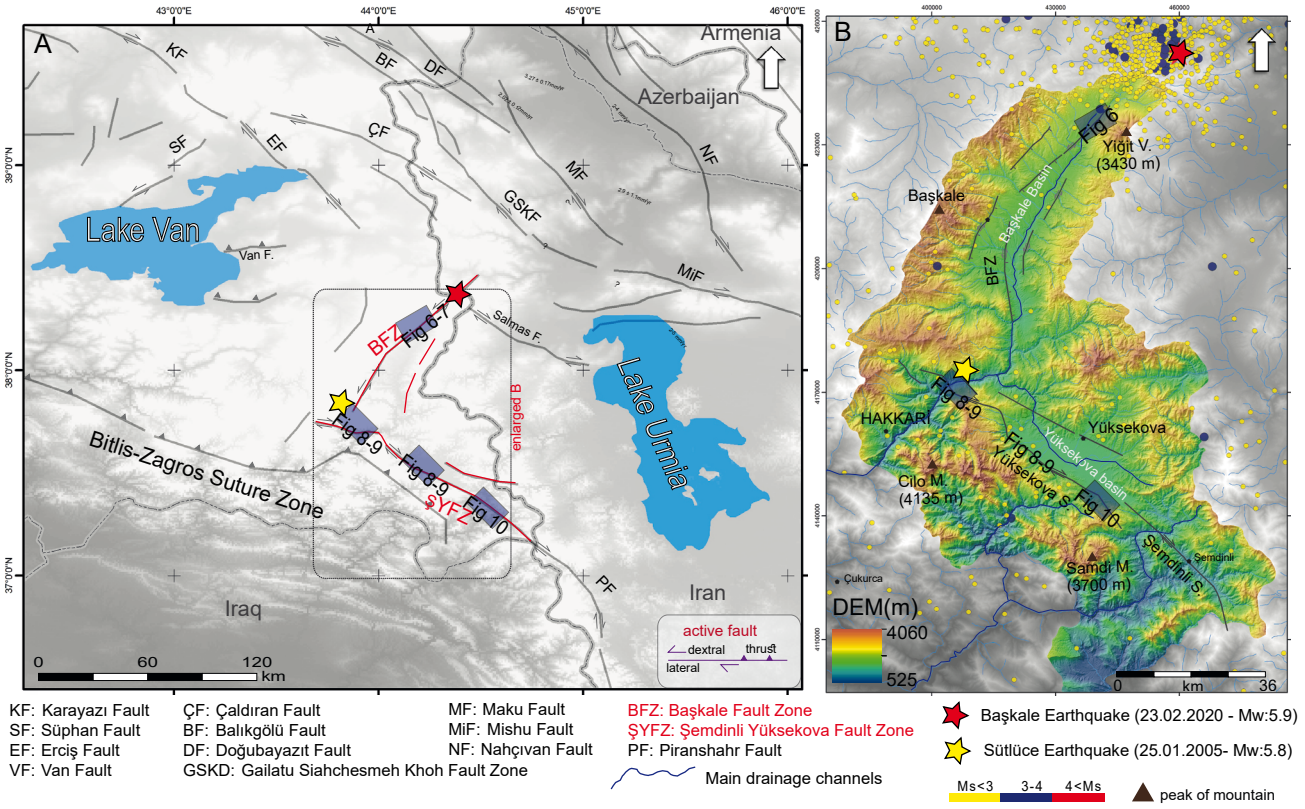

FIGURE 2. A) Spatial relationship between the Başkale Fault Zone and the Şemdinli-Yüksekova Fault Zone, both located within the East Anatolian province of shortening. B) Earthquakes recorded during the instrumental period within the study. The earthquake data used in this study were obtained from the 2024 records of the Earthquake Department of AFAD (Disaster and Emergency Management Authority).

(Fig. 2A, B). Historical earthquake records indicate that destructive earthquakes occurred on and around the BFZ in 1715 and 1851 (Ambrayeses, 2009). However, the available data for these eventsdo not sufficiently confirm the BFZ as the source of these events. The BFZ plays a crucial role in understanding the distribution of deformation in the region and has been responsible for significant earthquakes during the instrumental period. Notably, in 2020, this fault zone generated the devastating Başkale earthquake, located 5–10km north of the Turkey–Iran border (Başkale Earthquake: 23.02.2020, Mw= 5.9) (Fig. 2A, B)).

BFZ and ŞYFZ, and their immediate surroundings exhibit numerous seismic events recorded during the instrumental earthquake period, with magnitudes ranging between 5.0 <Mw< 6.0 (Fig. 2B). Due to the complexity of the tectonic structure in the region, multiple fracture systems could potentially host the Sütlüce Earthquake, resulting in a lack of consensus among the studies conducted (Atalay, 2007; Emre *et al.*, 2005; Koçyiğit, 2005). Koçyiğit (2005) posited that the Sütlüce Earthquake occurred along the BFZ, while Emre *et al.* (2005) suggested that this earthquake took place on the segment at the northwestern end of the ŞYFZ. An examination of both instrumental and historical earthquake data reveals that the BFZ exhibits greater seismic activity compared to the ŞYFZ.

The geological units exposed within the study area (Fig. 3) and its immediate surroundings have been classified and mapped into ten tectonostratigraphic units (Boray, 1975; Göncüoğlu and Turhan, 1984; Yılmaz, 1971, 1975; Ricou, 1971; Sağlam Selçuk and Düzgün, 2017; Sançar, 2018; Şenel, 2002, 2007).

The first unit consists of Permian-aged marbles and recrystallized limestones belonging to the Bitlis Metamorphics member. This geological unit crops out in the northwestern and southeastern parts of the study area. The second unit is a Jurassic–Cretaceous neritic limestone formation exposed in the southern part of the Yüksekova Basin. This unit also exhibits a concordant relationship with the fold axes of the BZSZ.

The third and fourth geological groups consist of Upper Cretaceous–Paleocene volcanosedimentary units and Upper Cretaceous ophiolitic rocks, respectively. These units are exposed between the BFZ and ŞYFZ. The fifth and sixth units are characterized by clastic and carbonate

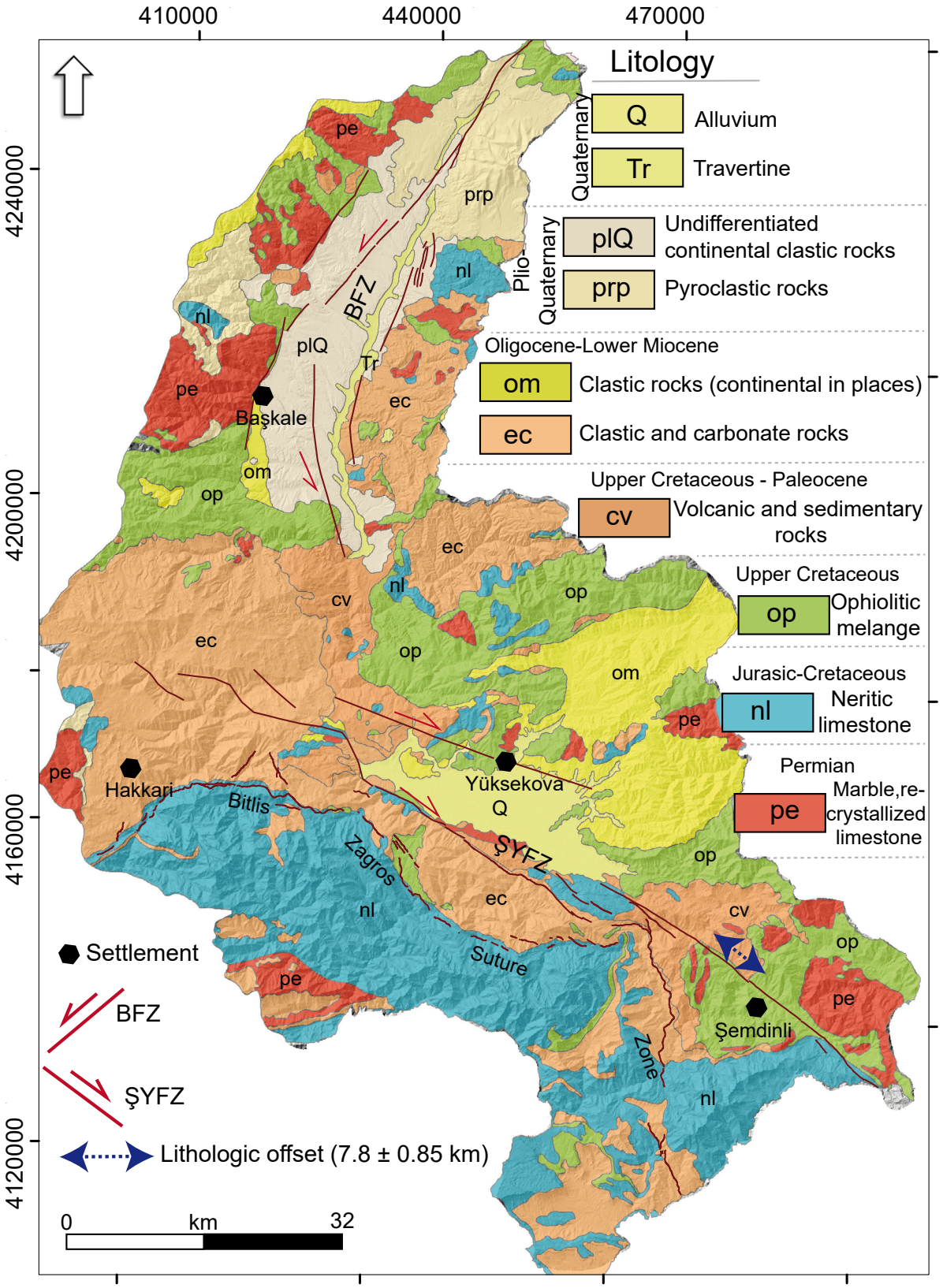

FIGURE 3. Geological map of the study region (The geological map was compiled based on the synthesis of the referenced sources) (Boray, 1975; Göncüoğlu and Turhan, 1984; Ricou, 1971; Sağlam Selçuk and Düzgün, 2017; Sançar, 2018; Şenel, 2002, 2007; Yılmaz, 1971, 1975). The dashed line with arrows at both ends indicates lithological offset. The displacement has been measured as 7.8±0.85 kilometers.

rocks such as sandstone, marl, and shale. These Oligocene–Miocene aged units crop out in the central parts of the study area. The Oligocene–Lower Miocene aged clastic and carbonate rocks (Şenel, 2002, 2007) are observed along a narrow zone between the fold axis of the BZSZ and the Yüksekova Basin.

The seventh and eighth lithological units, belonging to the Pliocene–Quaternary period, are undifferentiated clastic rocks and pyroclastic rocks. While pyroclastic rocks are located in the northeastern part of the study area, continental clastic rocks are widely distributed immediately west of the Başkale Basin. The most recent lithological units are travertines and alluvium. Travertines crop out in the northeastern and eastern parts of the Başkale Basin, whereas alluvial deposits form the basin floors of Yüksekova, Şemdinli, and Başkale. In particular, ridge travertines reflecting the activity of the BFZ are observed in the central part of the Başkale Basin.

To minimize the influence of lithological factors during morphometric index analyses, the evaluation was conducted based on the classification proposed by Selby (1980) (Fig. 3). In this classification, the study area is divided into five sub-classes ranging from very low to very high lithological resistance. Lithological units with very high resistance exhibit a heterogeneous distribution within the study area but are most commonly located in the northeastern and southern parts. Lithological units with high resistance are situated in the northeastern part of the Başkale District, while the least resistant lithological units are primarily found at the basin floors.

METHODOLOGY

Morphometric analyses are effective tools for quantitatively comparing and evaluating regions experiencing deformation and tectonic uplift (Keller and Pinter, 2002; Özsayın *et al.*, 2023). While a single index can be sufficient to identify drainage networks and basins influenced by tectonic processes, a combination of multiple indices is necessary to calculate the Index of Active Tectonics (IAT) (Chang *et al.*, 2015; Cheng *et al.*, 2016; Dehbozorgi *et al.*, 2010; El Hamdouni *et al.*, 2008; Esmaeil *et al.*, 2017; Kumar *et al.*, 2022; Pánek, 2004; Zygouri *et al.*, 2015). Although the IAT is typically applied to sub-basins influenced by a single fault (El Hamdouni *et al.*, 2008), in this study it was applied to basins (Fig. 4) affected by two distinct strike-slip fault systems—the ŞYFZ and the BFZ—in order to comparatively assess left- and right-lateral deformation in the region.

The morphometric analysis employed to calculate the IAT provided a quantitative basis for identifying tectonically driven anomalies, such as variations in valley and stream morphology, and for determining the influence of each fault zone on regional topography. In total, seven different indices were used to evaluate the tectonic activity of the ŞYFZ- and BFZ-controlled basins and to detect localized anomalies caused by tectonic processes. Unlike El Hamdouni *et al.* (2008), this study included the normalized steepness index (Ksn) and The Surface Roughness (SR) in the IAT calculation, while excluding the Basin shape index (Bs) due to its reduced sensitivity in basins that develop perpendicular to fault traces. Instead, the Asymmetry Factor (AF), which more clearly reflects slope aspect changes relative to fault orientation, was preferred. The SR index was also included in the IAT calculation for its effectiveness in capturing the degree of topographic deviation from planar surfaces, thereby serving as a proxy for deformation associated with fault zones.

Drainage networks and associated sub-basins were delineated for both fault zones using ArcMap 10.1 and MATLAB 2010. This approach ensured consistency in the morphometric analysis and enabled uniform comparison of tectonic impacts on drainage systems across the study area. The morphometric analysis was based on a high-resolution (10m) Digital Elevation Model (DEM) sourced from the Alaska Satellite Facility (https://search.asf.alaska.edu/#/). The seven morphomtric indices applied and integrated in the IAT are: Surface Roughness (SR), Hypsometric Integral (HI), mountain front Sinuosity (Smf), Valley floor width-to-height ratio (Vf), Asymmetry Factor (AF), Stream Length-gradient index (SL) and normalized steepness index (Ksn). These indices were selected based on prior studies (*e.g.* Bull, 1977; El Hamdouni *et al.*, 2008; Grohmann, 2004; Hack, 1973; Hobson, 1972; Keller and Pinter, 2002; Kirby and Whipple, 2012; Pérez-Peña *et al.*, 2010; Pike and Wilson, 1971; Silva *et al.*, 2003; Strahler, 1952; Wobus *et al.*, 2006).

AF values were calculated using the Raster Calculator in ArcGIS 10.1. SL and Ksn values were derived using the TecDEM toolbox in MATLAB (Shahzad and Gloaguen, 2011a, b). The Vf and Smf indices were computed using the 3D Analyst Tool in ArcMap, while hypsometric curves and integrals were generated with CalHypso software integrated into ArcGIS (Pérez-Peña *et al.*, 2009a, b). SR values were calculated using GRASS GIS 6.0.x on the 10×10 m DEM (GRASS Development Team, 2009; Grohmann, 2004a, b; Grohmann and Riccomini, 2009).

A total of 234 sub-basins associated with the ŞYFZ and BFZ were analyzed (Fig. 4). The resulting values were categorized based on their tectonic significance. To compute the IAT, the weighted scores of each index were summed and averaged. In this study, the classification was performed based on the methodology proposed by El Hamdouni *et al.*

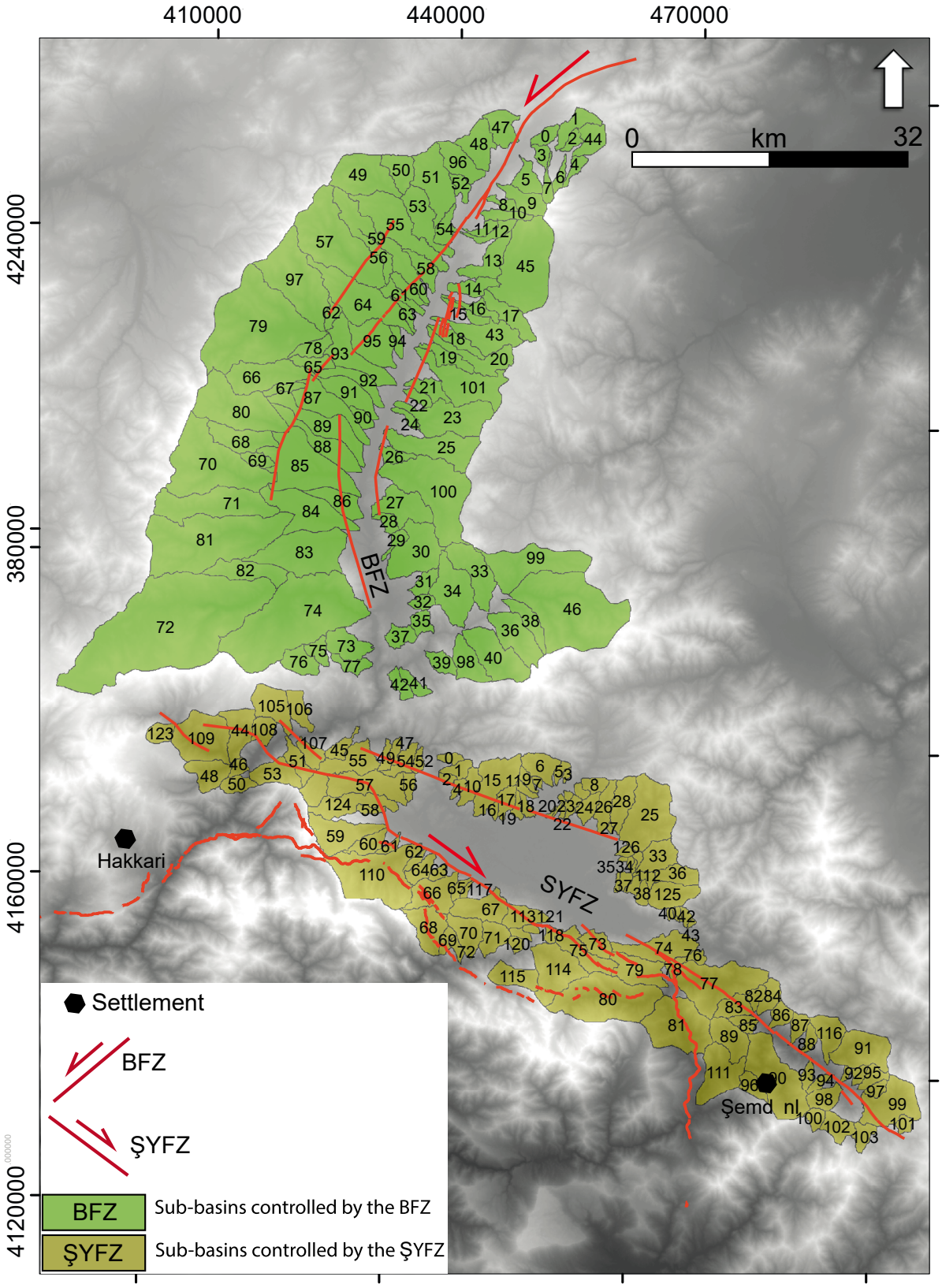

FIGURE 4. The regional location of the BFZ and ŞYFZ along with their main drainage networks (the blue dashed lines represent the main river network, while the red lines indicate active fault zones)."

(2008). The average value of each morphometric index was calculated for individual drainage basins. The IAT values were then categorized as follows:

1 <IAT< 1.5: Very high tectonic activity
1.5 <IAT< 2: High tectonic activity
2 <IAT< 2.5: Moderate tectonic activity
IAT> 2.5: Low tectonic activity

For the classification, the quantitative morphometric index values associated with the left-lateral strike-slip BFZ and the right-lateral strike-slip ŞYFZ were summed and averaged by dividing by the total number of indices used.

Ultimately, the IAT values provided a quantitative representation of the relative tectonic activity within basins influenced by the ŞYFZ and BFZ, enabling an assessment of deformation intensity and tectonic dynamics across the study area.

Drainage basin asymmetry

Drainage basins affected by regional tectonic deformation or localized deformational processes exhibit distinctive patterns, orientations, and geometric characteristics. The Asymmetry Factor (AF) is one of the simplest morphometric methods used to detect tectonically induced tilting at the scale of individual drainage basins (Giaconia *et al.*, 2012; Hare and Gardner, 1985; Keller & Pinter, 2002; Pérez-Peña *et al.*, 2010). AF is a morphometric index that quantifies the areal imbalance between the right and left halves of a drainage basin. This index enables a quantitative assessment of basin asymmetry caused by tectonic tilting or lithological contrasts (Hare and Gardner, 1985). It has been widely applied to evaluate tilt anomalies related to fault activity, deviations in drainage patterns due to lithology or climate, and to interpret basin evolution and geomorphological processes. The asymmetry factor is calculated using the following equation (Keller and Pinter, 2002):

Ar: the area of the right side of the drainage basin with respect to the downstream flow direction,
At: the total area of the drainage basin

In the study, the absolute function of basin-based asymmetry factor values was taken and these values (Giaconia *et al.*, 2012; Pérez-Peña *et al.*, 2010) were categorized into four classes: low symmetrical (AF< 5), moderately asymmetrical (5 <AF< 10), asymmetric basin (10 <AF< 15), and highly dominant asymmetric basin (AF> 15)

Stream length gradient

The Stream Length (SL) is an indicator of topographic discontinuities (slope changes) along the river channel and is influenced by factors such as lithological resistance to incision, tectonic movements, sea-level changes, and stream power. (Font *et al.*, 2010; Hack, 1973). The SL index, sensitive to variations in channel slope, can signify potential tectonic activity when there are no lithological differences along the stream profile (Keller and Pinter, 2002). SL index values are directly correlated with uplift rates, increasing in regions of active tectonics and decreasing in areas with comparatively low tectonic influence (El Hamdouni *et al.*, 2008; Keller and Pinter, 2002).

The SL index is calculated using the following formula (Hack, 1973; Keller and Pinter, 2002).

ΔH: Elevation difference within the stream segment (m).
ΔL: Horizontal length of the stream segment (m).
L: Total length of the stream from the source (m).

High SL values (SL> 300) can reflect active tectonic deformation, resistant lithology, and abrupt base level drops (DiBiase *et al.*, 2010; Hilley and Arrowsmith, 2008; Lamb and Fonstad, 2010). Conversely, low SL values (SL< 100) indicate balanced river profiles, softer lithological units, and low tectonic activity (Hack, 1973; Kirby and Whipple, 2012; Whipple and Tucker, 1999). Since the SL values calculated within the study area are associated with lithological units of moderate, high, and very high resistance, interpretations and classifications have been made based on the relative assessment of tectonic deformation.

The ratio of valley floor width to valley height

The Valley floor width-to-height ratio (Vf) is an important quantitative indicator used to understand fault movements or uplift rates. This ratio is calculated by dividing the width of the valley floor (the horizontal distance at the lowest part of the valley) by the total valley height (the vertical distance from the valley floor to the highest point of the valley walls) (Bull, 1977; Bull and McFadden, 1977). Low Vf values typically indicate narrow valley floors and deep valleys, often associated with U- or V-shaped valleys. Such valleys are usually found in tectonically active regions or relatively young valleys. In contrast, high Vf values reflect wide valley floors and relatively shallow valley depths. These values are generally observed in more mature valleys or areas where lateral erosion predominates (Bull and McFadden, 1977; El Hamdouni *et al.*, 2008; Keller and Pinter, 2002; Rockwell *et al.*, 1985; Silva *et al.*, 2003). The purposes of using the Vf index (Bull and McFadden, 1977; Keller and Pinter, 2002; Silva *et al.*, 2003) can be summarized as: i) quantifying the impact of tectonic activity on valley morphology, ii) evaluating the lateral and vertical components of deformation in fault zones and iii) distinguishing fluvial processes from tectonic deformation.

The Vf index is calculated using the following formula:
Vfw: Valley floor width (m)
Eld: Peak elevation of the left valley wall (m)
Erd: Peak elevation of the right valley wall (m)
Esc: Valley floor elevation (m)

A Vf value less than 1 indicates narrow and deep valleys, reflecting high tectonic uplift (Bull and McFadden, 1977; Khalifa *et al.*, 2018; Lavé and Avouac, 2001; Özsayın *et al.*, 2023; Rockwell *et al.*, 1985). Conversely, a Vf value greater than 1 corresponds to valleys of moderate width, indicative of low to moderate tectonic activity, as well as wide-based valleys reflecting tectonic quiescence (Blum and Törnqvist, 2000; Mutlu, 2025; Silva *et al.*, 2003).

Mountain-front sinuosity

The mountain front Sinuosity index (Smf), a parameter used to understand morphotectonic activity along a mountain front zone, measures the straightness or curvature of the mountain front line. It provides insights into the level of tectonic activity and is widely used in the geomorphological assessment of mountain fronts shaped by active faulting (Bull and McFadden, 1977; Keller and Pinter, 2002). An Smf value of 1 indicates a completely straight mountain front, which typically reflects high tectonic activity. In contrast, Smf values greater than 1 indicate a more sinuous mountain front, which is generally associated with decreasing tectonic activity or the dominance of incisional processes (Bull, 2007; Keller and Pinter, 2002; Pérez-Peña *et al.*, 2010; Rockwell *et al.*, 1985; Silva *et al.*, 2003)

The Smf index is calculated using the following formula:
Lmf: length of the steep mountain front (meters)
Ls: total mountain front length (meters)

The Smf is a function of both erosion and tectonic activity, and it varies depending on the uplift rate in the region (Rockwell *et al.*, 1985). Mountain fronts controlled by active faulting generally exhibit low Smf values; however, as the rate of uplift and/or tectonic activity decreases, erosional processes become dominant, resulting in higher Smf values (Bull, 2007; Keller and Pinter, 2002; Pérez-Peña *et al.*, 2010; Silva *et al.*, 2003). Therefore, mountain fronts associated with active uplift tend to be relatively linear, whereas a decrease or cessation in uplift allows erosional processes to progressively develop a more irregular and sinuous front. Low Smf values reflect straight mountain fronts, while high Smf values indicate increased sinuosity and irregularity. Specifically, Smf values lower than 1.4 represent linear mountain fronts shaped by recent tectonic activity along faults (Bull and McFadden, 1977). In contrast, higher Smf values imply a reduction in rock uplift rates and/or diminished fault activity along valley margins, allowing erosion to exert a more significant influence. Smf values exceeding 3 indicate tectonically inactive mountain fronts where erosion dominates and the actual fault trace may lie more than 1 km away from the current mountain front.

Hypsometric integral

The Hypsometric Integral (HI) is a dimensionless morphometric parameter that quantitatively describes the elevation distribution of a drainage basin or topographic surface and is commonly used to determine the stage of landscape evolution and the level of tectonic activity (Strahler, 1952). The HI value is calculated using the ratio between the mean elevation of a unit area and the difference between its maximum and minimum elevations (Keller & Pinter, 2002):
h: Mean elevation;
hmin: Minimum elevation;
hmax: Maximum elevation

The HI value ranges between 0 and 1 and provides indirect insights into the degree of erosion, topographic maturity, and tectonic activity of a landscape. Hypsometric integral values greater than 0.5 (HI> 0.5) indicate that the basin is youthful. In contrast, values lower than 0.3 (HI< 0.3) suggest that the basin is old and has undergone significant erosion. If the HI value falls between 0.3 and 0.5 (0.3 <HI< 0.5), it indicates that the basin has reached a mature stage and is in a state of equilibrium (Pike & Wilson, 1971; Willgoose, 1994; Keller & Pinter, 2002). In this context, high HI values generally point to regions controlled by active tectonic processes that have not yet reached a graded profile due to the limited influence of external morphodynamic agents (El Hamdouni *et al.*, 2008). The hypsometric integral is also related to the area under the hypsometric curve, which is a graphical representation of normalized elevation plotted against normalized area. The shape of the curve reflects the stage of landscape development: upward-convex (concave) curves are associated with high HI values and thus represent youthful topography, whereas downward-convex curves correspond to low HI values and highly eroded terrains (Keller & Pinter, 2002; Strahler, 1952).

In recent years, HI analysis has been effectively applied in Geographic Information Systems (GIS) environments using DEM data. This approach allows HI values calculated across different segments or basins to be widely used in assessing relative tectonic activity along active fault zones (El Hamdouni *et al.*, 2008; Mutlu, 2025; Silva *et al.*, 2003).

Surface Roughness

Surface Roughness (SR) measures the deviation of a surface from a perfectly planar form. In this metric, flat

surfaces are represented by values close to 1, whereas irregular surfaces exhibit higher values. Surface roughness, which is highly sensitive to topographic dissection, incision, and faulting, tends to increase with the intensification of fluvial erosion (Andreani and Gloaguen, 2016; Andreani *et al.*, 2014; Day, 1979; Grohmann, 2004a, b; Hobson, 1972; Pike and Wilson, 1971; Zebari *et al.*, 2019). Topography controlled by active faults can be effectively distinguished using this index (Zebari *et al.*, 2019). Surface roughness is an important parameter for morphological segmentation (Grohmann, 2004a), and it is widely used in the identification of karstic terrains, the morphological characterization of lake sediments, structural subdivision of sedimentary basins, morphometric analyses of alkaline massifs, structural assessment of strike-slip shear zones, and in delineating macro-geomorphological boundaries (Day, 1979; Ferrari *et al.*, 1998; Grohmann *et al.*, 2007; Hakanson, 1974; Karmann *et al.*, 1996; Steiner *et al.*, 2006; Zebari *et al.*, 2019).Surface roughness is calculated using the following equation (Grohmann, 2004a, b; Hobson, 1972):

where TS represents the actual surface area (m^2), and FS refers to the projected planar area of the surface (m^2).

The surface roughness values were computed using a 10×10m resolution DEM within the GRASS GIS 6.0.x environment (GRASS Development Team, 2009; Grohmann, 2004a, b; Grohmann and Riccomini, 2009). In this study, stream incisions shaped by tectonic influences are used as a numerical indicator of relative tectonic activity, as they reflect the relative tectonic relationships among different basins through elevated surface roughness values. A quantitative assessment was conducted by comparing the SR values obtained from the Başkale, Yüksekova, and Şemdinli basins, which are controlled by the BFZ and ŞYFZ. These SR values were used as classification inputs within the IRAT framework. High SR values were interpreted as indicators of active tectonics.

Normalized channel steepness index

Normalized channel steepness index (Ksn) is a geomorphic metric used to estimate the rate of tectonic deformation along active faults and to detect disequilibrium in landscape morphology, such as uplift or erosion (Kirby and Whipple, 2012; Özsayın *et al.*, 2023). Ksn is an effective parameter for identifying slope anomalies along river longitudinal profiles (Ouimet *et al.*, 2009; Whittaker, 2012). In a typical drainage basin, river gradient generally decreases progressively from the headwaters downstream. However, this pattern may be disrupted by vertical displacements associated with active faulting or by lithological transitions with differing resistance to erosion.

In graded streams, the relationship between channel Slope (S) and upstream drainage Area (A) is described by a power-law function, initially proposed by Hack (1957):

$S = ksA^{-Q}$

S: Local channel slope ($S = \Delta h/\Delta x$)

A: Drainage area upstream of the point (km^2)

θ: Concavity index that describes the relationship between channel slope and drainage area (commonly assigned a fixed value, *e.g.* 0.45).

In this equation, Ks represents the channel steepness index, while θ denotes the concavity index (Flint, 1974). Factors such as bedrock lithology, active tectonic processes, and climatic conditions directly influence channel slope and basin area, thereby affecting the values of Ks and θ (Kirby and Whipple, 2012; Wobus *et al.*, 2006).

Regression analyses based on log–log slope–area plots are frequently employed to estimate Ks and θ values (Ferrater *et al.*, 2015). These plots also play a critical role in identifying knickpoints —sudden changes in slope— and geomorphic regions with varying uplift rates (Burbank and Anderson, 2013; Kirby and Whipple, 2012; Whipple *et al.*, 2013; Wobus *et al.*, 2006). The formation of knickpoints is typically attributed to abrupt changes in boundary conditions, such as base-level shifts or climatic fluctuations (Bishop *et al.*, 2005; Kirby and Whipple, 2012; Snyder *et al.*, 2003). Previous studies have shown that the concavity index (θ) commonly ranges between 0.4 and 0.6, and is relatively less sensitive to tectonic activity, lithological variability, or climate change (Kirby and Whipple, 2012; Whipple *et al.*, 2013). In this study, the channel steepness index (Ksn) was calculated using TecDEM, a MATLAB-based toolbox integrated with TopoToolbox. The calculation process involved the following steps: importing DEM data, extracting the drainage network, computing slope (S), defining the concavity index (θ), calculating Ksn, and finally visualizing the results. In TecDEM and similar tools, θ is commonly set to a constant value of 0.45. This approach is justified by several reasons: i) θ= 0.45 is consistent with the stream power erosion model, which reflects the theoretical equilibrium of channel profiles (Whipple and Tucker, 1999); ii) this value has produced consistent results in various global studies (*e.g.* Himalayas, California) (Wobus *et al.*, 2006); iii) using a fixed θ allows for more reliable comparisons across different regions; iv) allowing θ to vary can introduce uncertainty and obscure tectonic signals (Kirby and Whipple, 2012) and v) a fixed θ eliminates the need for complex regression analyses and reduces processing time. For these reasons and in line with general practice in the literature, θ was set at 0.45 in this study.

In addition to morphometric analyses, observable neotectonic structures and fault displacements affecting

the morphology were also measured. Each segment of the ŞYFZ and BFZ was examined individually, and the fault displacements were identified using both orthophotos with a resolution of 30 centimeters and a 1m cell size digital terrain model derived from these orthophotos. The orthophotos were processed into a digital terrain model using Agisoft Metashape software. In areas not covered by orthophotos, 5-meter resolution DEMs were generated using contour lines. In areas lacking topographic contour lines, 10-meter resolution DEM data obtained from the open-access platform (https://search.asf.alaska.edu/#/) were utilized. Morphometric indices were calculated based on this DEM. For displacement measurements, an error margin corresponding to 11% of the measured offset length was assumed, regardless of scale and resolution (Gold *et al.*, 2009, 2011). The displacements along the BFZ were measured using orthophotos acquired in 2015. Offset features along the ŞYFZ were analyzed based on a 1-meter resolution Digital Surface Model (DSM).

RESULTS

In the study area located in southeasternmost Turkey, seven morphometric analyses were applied along the BFZ and ŞYFZ to determine the relative active tectonic indices of these two fault zones. In addition, morphotectonic features were mapped using aerial and satellite imagery, and the interpretations were supported with field-based observations and high-resolution topographic data.Major Neotectonic Features, General Drainage Characteristics and Displacements.

The study area, located in the Southeastern Anatolia Region and characterized by a rugged and mountainous topography, is bounded by Lake Van (1647m) to the northwest, Lake Urmia (1268m) to the Northeast, and the Tigris River (247m) to the South (Fig. 5). The Cilo-Sat Mountains, located in the southeastern part of Yüksekova district, represent the second highest peak in Turkey, with an altitude of 4,135 meters. The glacial features in the region, including valley-type and cirque glaciers, are situated between elevations of 2,800m and 4,135m, with Uludoruk Summit (4,135m) being the highest point. The Zap River and its tributaries, which form the primary drainage network in the region, have deeply incised the landscape, creating narrow and steep-sided valleys. The Zap River, controlled by the BFZ, exhibits a higher-energy drainage network, whereas the Nehil streams, controlled by the ŞYFZ, display lower-energy fluvial characteristics. These two drainage systems converge to the north of the Cilo-Sat Mountains, subsequently joining the Greater Zab River and eventually merging with the Tigris River (Fig. 4). The Altınsu stream, controlled by the southeastern branch of the ŞYFZ, flows southeastward and drains into the Rubar Barazgird River. Subsequently, this stream also reaches the Tigris River through its connection with the Greater Zab River (Fig. 4).

When examining the regional morphology, the highest peak is the glacier-capped Cilo-Sat Mountain (4135m). Along with Cilo Mountain, the high peaks extend parallel to the BZSZ. North of the BZSZ, strike-slip faulting trending NW-SE and NE-SW is observed, whereas to the south of the BZSZ, E-W oriented folds are distinctly reflected in the topography (Fig. 4). Between these two tectonic regimes lies the Zap River, which drains the catchment towards the Tigris River (Fig. 4). Since the study area is located north of the BZSZ, it exhibits similar morphological elevations as well as comparable climatic characteristics to those of the Lake Van Basin (TSMS, 2025).

The study area is located in the southeasternmost part of Eastern Anatolia, the region with the highest average elevation in Turkey. The region situated between Lake Van and Lake Urmia hosts both the BZSZ and the Cilo (Sat) Mountains, and is characterized by a complex topography —including abrupt slope changes, flat plains, and steep elevations coexisting within short distances— as well as a highly intricate drainage network, where sudden shifts in stream directions are commonly observed (Fig. 4)According to long-term data (1961–2024) recorded at the Hakkari Meteorological Station, the annual average temperature in the region is 10.4°C. The highest average temperature, 31.2°C, was recorded in August, while the lowest, -0.2°C, occurred in January (TSMS, 2025). Precipitation data indicate that the highest monthly average rainfall, 126.6mm, occurred in March, while the lowest, 4.6mm, was observed in August. The region's annual average precipitation is 748.5mm (TSMS, 2025). Examination of the climatic data for the study area shows that, despite minor local-scale variations influenced by geographical location, the region generally reflects the typical continental climate characteristics of eastern Anatolia.

While the BFZ controls the Zap River, which flows southward through a narrow valley, the ŞYFZ controls both the Nehil River, which flows northwestward through a broader plain, and the Altınsu River, which flows southeastward through a V-shaped valley. The BFZ, which stands out within EAPS where right-lateral strike-slip faults generally dominate, controls the Başkale Basin from both its western and eastern margins. The western part of the basin exhibits a more rugged and sharply defined topography, whereas the eastern part is characterized by a gentler slope and a less inclined morphology (Fig. 4). A total of 236 sub-basins associated with the ŞYFZ and the BFZ were analyzed (Fig. 5). Specifically, morphometric indices were applied to 131 sub-basins controlled by the ŞYFZ and 105 sub-basins influenced by the BFZ. In addition, both point-

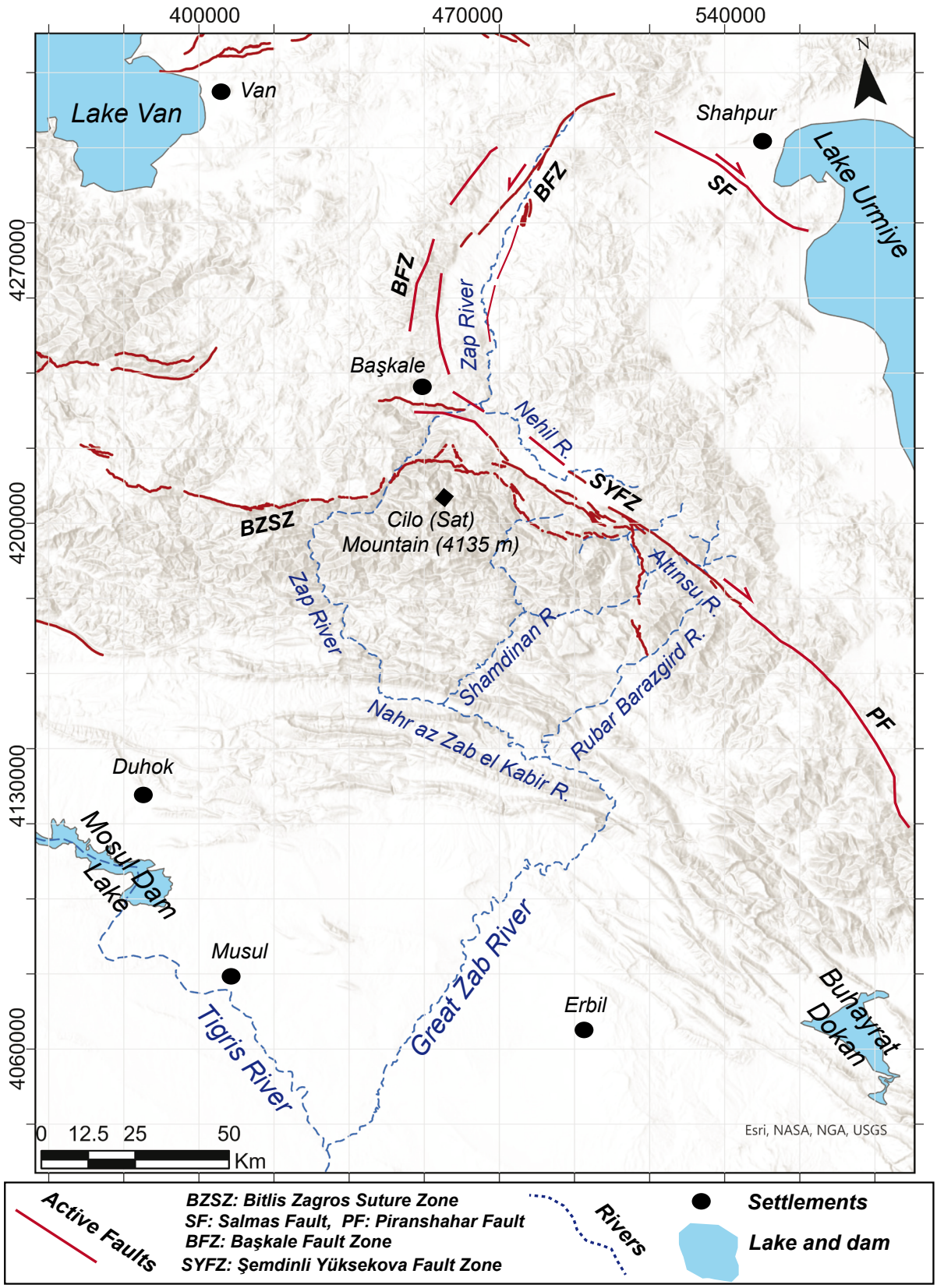

FIGURE 5. General view of the sub-basins controlled by the BFZ and SYFZ, along with the overall distribution of active faults (BFZ: Başkale Fault Zone, SYFZ: Şemdinli-Yüksekova Fault Zone).

based and linear morphometric indices were applied along the trace of each fault zone (Fig. 5).

Numerous morphotectonic structures and fault offset are present along the BFZ (Fig. 6). At the northeastern end of the BFZ, offset streams and elongated ridges, which are disrupted by the fault, are clearly delineated (Fig. 6; 7). The ridges extending parallel to the fault trace have been observed to the north of Bilgeç Village (Fig. 6A) and to the northeast of Özpınar Village (Fig. 6B). To the north of Bilgeç Village, a ridge trending N52°E extends approximately 300 meters in length (Fig. 6A, C). Immediately to the southwest of this ridge, another ridge with the same orientation is present, measuring about 90 meters in length (Fig. 6A). To the northeast of Özpınar Village, a ridge trending N50°E has been measured to be 270 meters in length (Fig. 6B).

Offsets of 192±21.1m, 46±5.06m and 80±8.8m were measured in stream channels displaced by the BFZ (Fig. 7). The 192±21.1m stream offset was measured in the northeastern segment of the BFZ, between Özpınar and Güvendik villages (Fig. 7A, D). The 46±5.06m and 80±8.8m stream offsets were measured immediately east of Özpınar Village (Fig. 7B, C). This location also corresponds to the village that experienced the most severe damage during the Mw 5.9 earthquake that occurred on February 23, 2020.

Compared to the BFZ, the ŞYFZ provides more pronounced indicators in terms of both morphology and stream offsets. The most prominent morphotectonic feature of the ŞYFZ is the Yüksekova Basin (pull apart basin) (Figs. 8A; 9A). In particular, a sharp linear boundary is observed between the western part of the basin and the fault trace (Fig. 8A). In the locations where the fault trace was followed, geomorphic markers such as triangular facets and the abrupt termination of a newly developed terrace due to fault activity (fault scarp) were identified (Fig. 8A, C). A cumulative offset of 513±56.43 meters was measured at the northwestern tip of the ŞYFZ, near Yuvalı Village, where a stream channel and a ridge exhibit an abrupt change in slope (Fig. 8B).

At the northwesternmost edge of the Yüksekova Basin, a stream offset of 89±9.46 meters was identified through field investigations along the ŞYFZ, north of Armutdüzü Village (Fig. 9B). This location also marks the initiation point of the fault scarp, where a slope surface developed parallel to the fault trace at an elevation of 2521 meters, forming a pronounced topographic threshold that abruptly descends to an elevation of 1570 meters (Fig. 9B). At this location, a well-preserved paleo-landslide morphology is also evident, initiating on the fault-controlled piedmont surface and extending downslope (Fig. 9B).

Numerous systematically developed offsets are present along the ŞYFZ (Fig. 10). The following stream offsets have been measured along the area: the central part of the Yüksekova Basin, immediately east of Gürdere Village, sequential stream offsets of 62±6.8m, 66±7.2m, and 95±10.4m (Fig. 10A). Southeast of Gürdere Village, near Karlı Village, stream offsets of 145±15.9m, 96±10.5m, and 150±16.5m (Fig. 10B); Southeast of these measured offsets, near Çatma Village, stream offsets of 205±22.5m and 65±7.1m (Fig. 10C). A stream offset measuring 77±8.47meters was identified northwest of Kamışlı Village along the fault trace (Fig. 10D). The ŞYFZ can be distinctly and sharply traced in the field, on digital surface models, and satellite imagery. Numerous morphological indicators have been detected and mapped, particularly in the central and southeastern segments of the ŞYFZ. This fault, considered a seismic gap, clearly shows tectonic activity confirmed through morphological and field data. Geological mapping studies conducted in the study area have identified a 7.8±0.85km right-lateral offset along the ŞYFZ, providing lithological evidence for its neotectonic activity (Fig. 3). This deformation is morphologically and stratigraphically pronounced by the sharp right-lateral displacement of Upper Cretaceous-Paleocene volcano-sedimentary units and Upper Cretaceous ophiolitic rocks. In particular, the linear features developed parallel to the fault zone in the southeastern segment of the ŞYFZ reflect the long-term slip kinematics and the cumulative displacement amount of the fault.

Drainage basin asymmetry

According to the AF index calculations performed in the sub-basins controlled by the ŞYFZ, there are 41 dominant asymmetric basins, 25 moderately asymmetric basins, 34 slightly symmetric basins, and 27 symmetric basins (Table I, Appendix). According to the AF index calculations conducted (Fig. 5; Table I) in the sub-basins controlled by the BFZ, there are 19 dominant asymmetric basins, 33 moderately asymmetric basins, 20 slightly symmetric basins, and 30 symmetric basins (Table II). The highly asymmetric sub-basins identified along the BFZ (Fig. 5; Table II) are predominantly located in the eastern sector of the basin. In contrast, asymmetric basins in the Şemdinli-Yüksekova Basin are mainly concentrated in its western part, where the thrust component of the fault is more dominant (Fig. 11A).

The AF index, widely used in active fault zones, is a morphometric parameter that helps to assess whether drainage systems have developed under tectonic control in alignment with the regional tilting direction. However, it is important to note that AF values are influenced not only by tectonic activity but also by lithology and the mechanical strength of the lithological units.

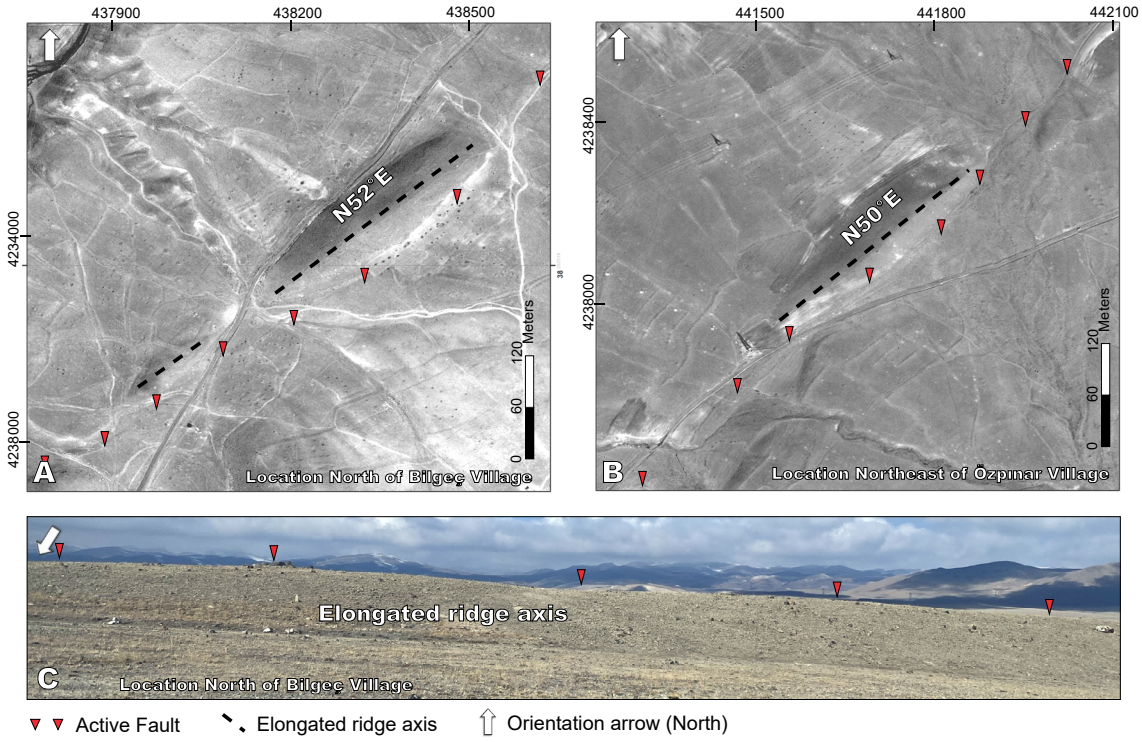

FIGURE 6. General view of the elongated ridges located in the northeastern part of the BFZ (around Özpınar and Bilgeç villages) on the 2015 orthophoto (Black dashed lines indicate the axis of the ridge, and red triangles represent the BFZ). A) Elongated ridge developed parallel to the fault trace, north of Bilgeç Village. B) Elongated ridges observed in the northeastern part of Özpınar Village, aligned parallel to the fault trace. C) Field photograph of the elongated ridge observed north of Bilgeç Village, aligned parallel to the fault trace.

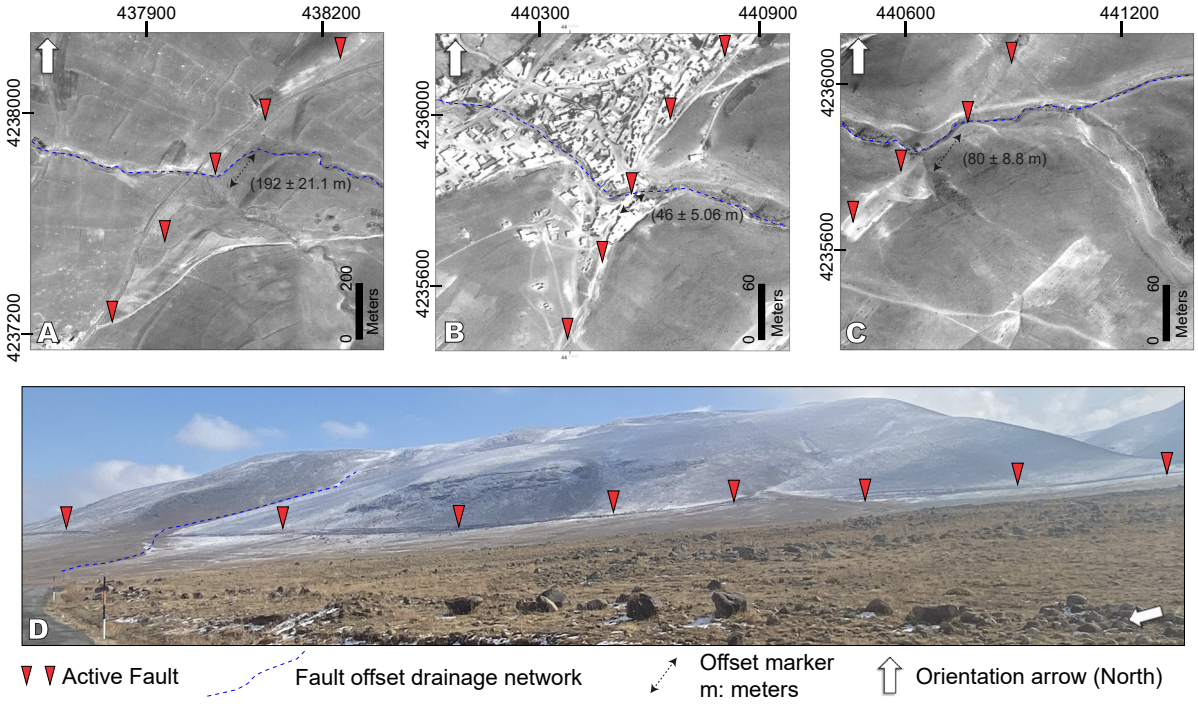

FIGURE 7. General view of the fault offset located in the northeastern part of the BFZ (around Özpınar) on the 2015 orthophoto (Red triangles with black borders represent the BFZ, The stream channels are represented by blue dashed lines, Stream offsets are marked by black dashed lines with bidirectional arrows.) A) Orthophoto showing the 192 ± 21.1 meter offset of the stream channel measured northeast of Özpınar Village.B) Orthophoto showing the 46 ± 5.06 meter offset of the stream channel measured in the center of Özpınar Village. C) Orthoimage showing the 80 ± 8.8 meter offset of the stream channel measured east of Özpınar Village. D) Field photograph showing the 192 ± 21.1 meter stream offset measured to the northeast of Özpınar Village.

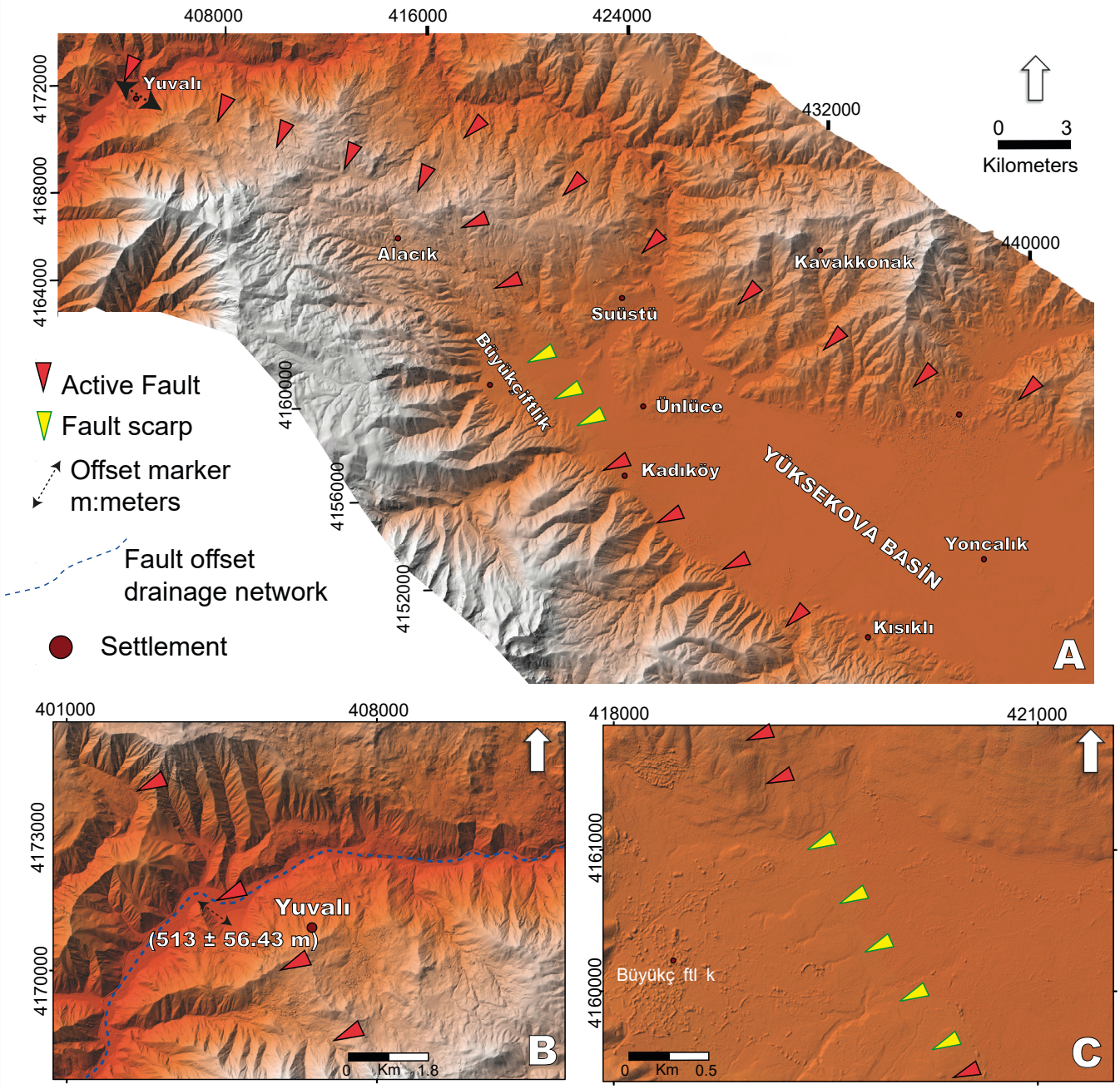

FIGURE 8. Morphotectonic indicators of the northwestern segment of the Şemdinli–Yüksekova Fault Zone. A) Fault lineament expression on the 1-meter resolution Digital Surface Model,; B) View of the 513±56.43-meter dextral/lateral offset identified on the Digital Surface Model (DSM) near Yuvalı Village, located at the northwestern tip of the ŞYFZ; C) Fault scarps observed near the village of Büyükçiftlik.

The Bitlis metamorphics within the study area are primarily composed of schist, phyllite, and Permian-aged marble and recrystallized limestone (Boray, 1975; Sançar, 2018). The volcanic units in the region include basaltic and granitic lithologies (Şenel, 2002, 2007). Considering their physical characteristics and hardness levels, these volcanic and metamorphic rocks are classified as high-strength rocks according to Selby's (1980) classification. In this context, the high and very high AF values measured in the resistant zones located in the southeastern part of the study area indicate that the drainage systems are largely controlled by fault activity rather than having reached a state of equilibrium. This strongly suggests that basin asymmetry in these regions primarily reflects tectonic forcing. Based on the conducted analysis, 19 strongly asymmetric sub-basins were identified in the Başkale Basin and 41 in the Yüksekova Basin.

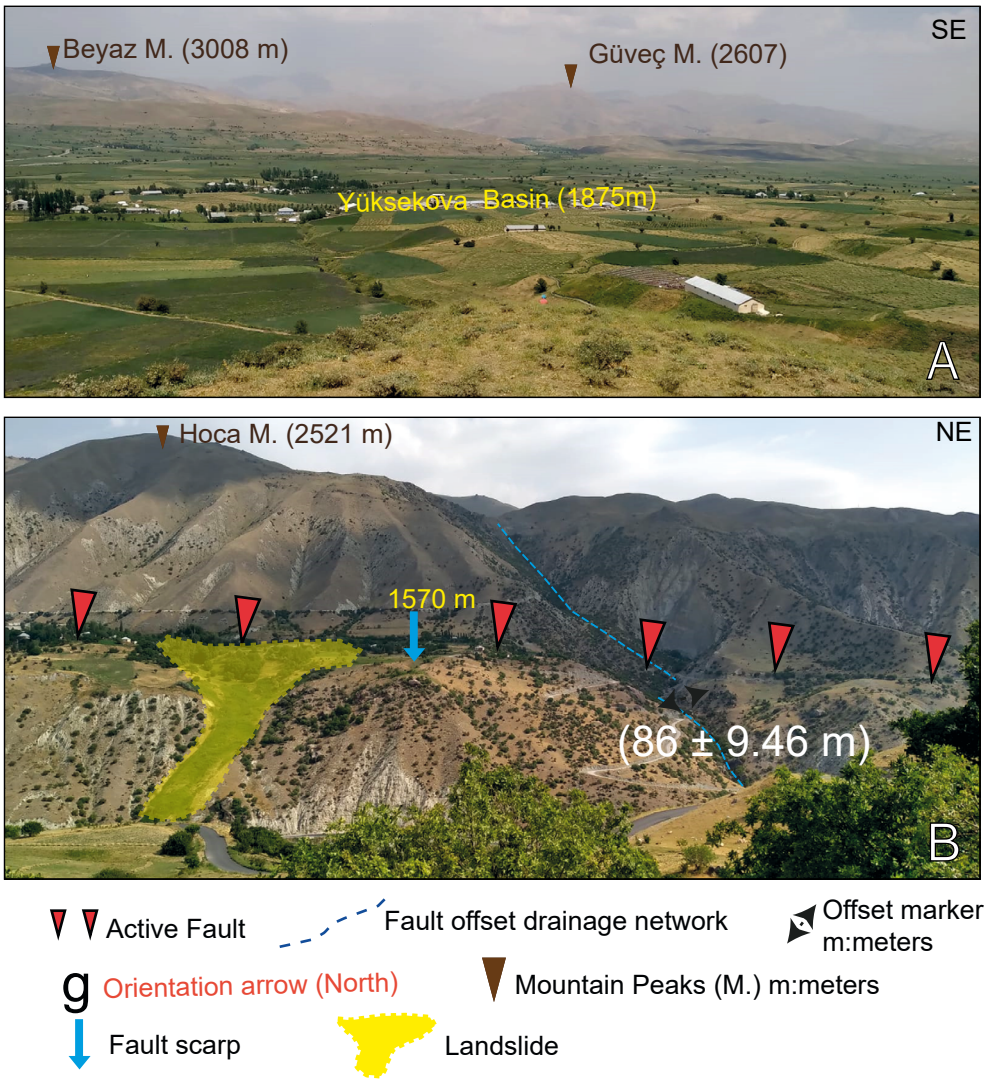

FIGURE 9. Terrain view of the Şemdinli-Yüksekova Fault Zone. A) Overview of the Yüksekova Basin as a pull-apart basin influenced by the Şemdinli-Yüksekova Fault Zone; B) Displacement and landslide development at the northwestern end of the SYFZThe numbers written in white, (89±9.46 m), indicate the stream offset measured in meters, The blue dashed lines represent the stream network, The blue arrow indicates the fault scarp.

Based on the calculated AF values, the BFZ is classified as second-degree in terms of tectonic activity, whereas the ŞYFZ falls into the first-degree category. This classification is derived from the average AF values calculated for each basin (Tables 1; I; II).

Stream length gradient

SL index values were computed for the streams controlled by both fault zones (Fig. 11B; Table III). The resulting SL index values exhibit a range from 60 to 4000. The highest SL index value obtained along the BFZ was measured as 1038 in the western part of the basin, specifically within and to the northwest of the Başkale District. In contrast, values as high as 4000 were recorded on the Şemdinli-Yüksekova Fault Zone. The values were primarily obtained from sudden abrupt changes observed on the Yeniışık segment. Additionally, the topographic changes between the ŞYFZ and the BZSZ produced an SL index value of 3800. The areas exhibiting high SL index values along the Başkale Fault Zone correspond to Mesozoic-aged metamélange units characterized by uniform lithology, with no observable variation in geological units. According to Selby's (1980) classification, these units are considered high-strength rocks. These units, located to the west of the Başkale basin, have the highest values of the Başkale basin with an SL value of 1000 (Fig. 11B). On the Şemdinli Yüksekova Fault Zone, the maximum SL values were obtained from the Eocene-Oligocene pebble-sandstone-mudstone units situated in the northwestern part of the Yüksekova Basin, exhibiting index values approaching

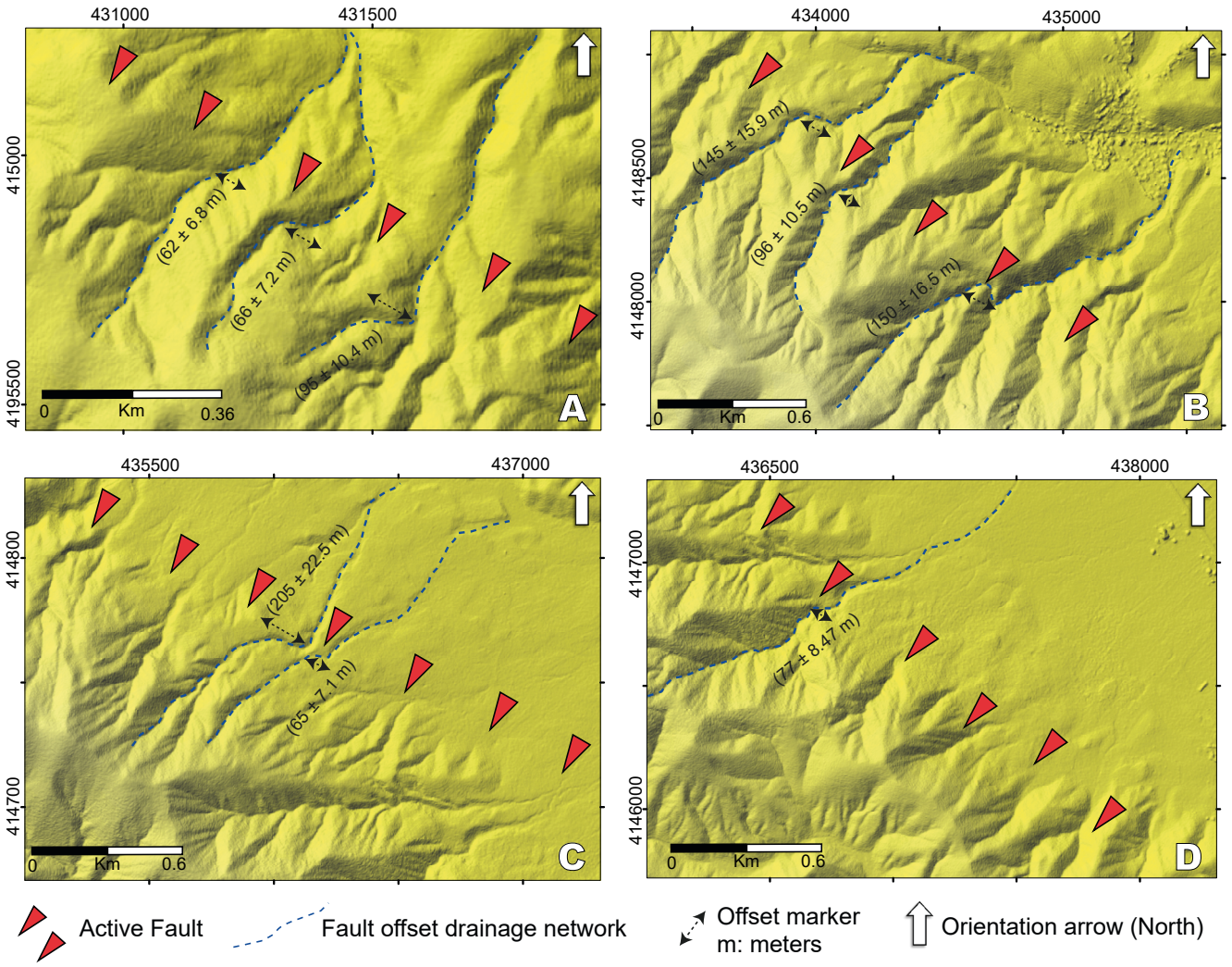

FIGURE 10. The view of the measured displacements in the middle part of the Şemdinli-Yüksekova Fault Zone (ŞFYZ) on a 1-meter resolution Digital Surface Model (DSM). A) The appearance on the DSM of the measured offset of 62±6.8m, 66±7.2m and 95±10.4m near Gürdere Village. B) The appearance on the DSM of the measured displacements of 145±15.9m, 96±10.5m and 150±16.5m south of Karlı Village. C) The DSM view of the measured displacements of 205±22.5m and 65±7.1m southeast of Çatma Village. D) View of the 77±8.47m offset measured northwest of Kamışlı Village on the 1-meter resolution DSM (Red triangles indicate the locations of active faults, the dashed, arrow-headed lines at both ends represent displacement locations, the dashed blue lines indicate segments of the drainage network affected by displacement.

4000. With the analysis of the highest SL values in the Yüksekova and Başkale basins, ıt is found that the Yüksekova Basin's values are, on average, about three times higher than those observed in the Başkale Basin. The SL index values derived from the study were categorized into five distinct classes (Fig. 11B). A special classification was conducted by calculating the average weights to assess the contribution of SL index values to the relative tectonic activity index for both fault zones. SL index measurements were conducted on 139 river channels located within the BFZ. In the Başkale Basin, which has SL values ranging from 10.24 to 1039, values of 400 and above were recorded in 20 river channels. The highest values are generally located in the northwest of the Başkale Basin. The average SL value obtained in the Başkale Basin is 172.53. SL index measurements were conducted on 574 river channels located within the ŞYFZ. In the Yüksekova and Şemdinli basins, which have SL values ranging from 1.2 to 5049, values of 400 and above were recorded in 168 river channels. The highest values are generally found at the northwestern end of the ŞYFZ. The average SL value obtained in the Yüksekova and Şemdinli basins is 428.05. Since the classification was focused on fault zone-specific evaluation, the average SL values obtained for the BFZ and the ŞYFZ were used as the basis for comparing the relative tectonic activity levels of the two fault systems. According to the weighting degrees, the BFZ was classified as Class 3, while the ŞYFZ was classified as Class 1.

The ratio of valley floor width to valley height

To clearly illustrate the elevation distribution within both fault zones, Vf values (valley floor width to height ratio) were obtained from a total of 78 points, ranging between 0.13 and 2.7. The Vf index was calculated along both the BFZ and the ŞYFZ in lithologically homogeneous areas and at locations perpendicular to the fault strike. In these calculations, geomorphological features such as fault lineaments, fault scarps, slope breaks, and fault-controlled valleys were taken into account. The selected points represent cross-sections of transverse valleys along streambeds.

Measured Vf values in the Başkale Basin vary between 0.28 and 2.7 (Fig. 12B). Low Vf values indicating V-shaped valleys (values close to 0) were recorded primarily in the S1, S2, and S6 segments of the basin. Notably, the S1 segment with a Vf value of 0.28 represents the area with the highest degree of tectonic dissection within the Başkale Basin (Fig. 12B). In the Yüksekova Basin, Vf values range from 0.13 to 1.48 (Fig. 12B). The S1, S5 and S6 segments exhibit the most prominent tectonic indicators among the measured values. Particularly, the Yüksekova S1 segment, with a Vf value of approximately 0.13, represents V-shaped valleys developed under strong tectonic control.

When comparing the Vf values calculated for both fault zones, the average Vf value for the BFZ is 0.99, whereas the average Vf value for the ŞYFZ is 0.36. Based on these quantitative values, the BFZ is classified within the third tectonic class, while the ŞYFZ is categorized as first tectonic class in terms of Vf values (Table 1).

Mountain-front sinuosity

In addition to the Vf values, Mountain-front sinuosity (Smf) values were also calculated for both fault zones (Fig. 12A, C). The Smf index, utilized to identify mountain fronts exhibiting active tectonics (Bull and McFadden, 1977; Keller and Pinter, 2002), was analyzed across 12 sub-segments. In the calculation of Smf values, geometric segmentation was applied, with particular attention given to segments that exhibit a clear mountain front and well-defined slope breaks. For the BFZ, six segments were selected where a distinct morphological boundary exists between the flat plains and mountainous areas. Four of these segments are located in the northwestern part of the Başkale Basin, while two are situated in the southeastern part. Similarly, for the ŞYFZ, six segments were selected based on clear morphological contrasts between the plains and the adjacent mountainous terrain. Five of these segments control the Yüksekova Basin, whereas one segment controls the Şemdinli Basin. In the Yüksekova Basin, three segments are located in the southeastern part, and two in the Northern part, for Smf calculation.

The Smf index of the segments of the Başkale fault zone, presents values between 1.06 and 1.26. The segments S1 and S6 of Başkale are notable for their pronounced active mountain fronts (Fig. 12C). In contrast, Smf values in the Şemdinli-Yüksekova fault zone range from 1.06 to

Table 1. The morphometric index values calculated for the basins controlled by the Başkale Fault Zone (BFZ) and the Şemdinli-Yüksekova Fault Zone (ŞYFZ), along with their corresponding Index of Active Tectonics (IAT) values, are as follows

Geomorphic Index	BFZ	ŞYFZ	BFZ Class	ŞYFZ Class
SR	2,33	3,46	2	2
HI	0,45	0,47	1	1
VF	0,99	0,36	3	1
Smf	1,14	1,11	1	1
AF	35	41	2	1
SL	1038	4000	3	1
Ksn	<300	>600	2	1
IAT	Middle	High	2	1,14
	2<IAT<2,5	1<IAT<1,5		

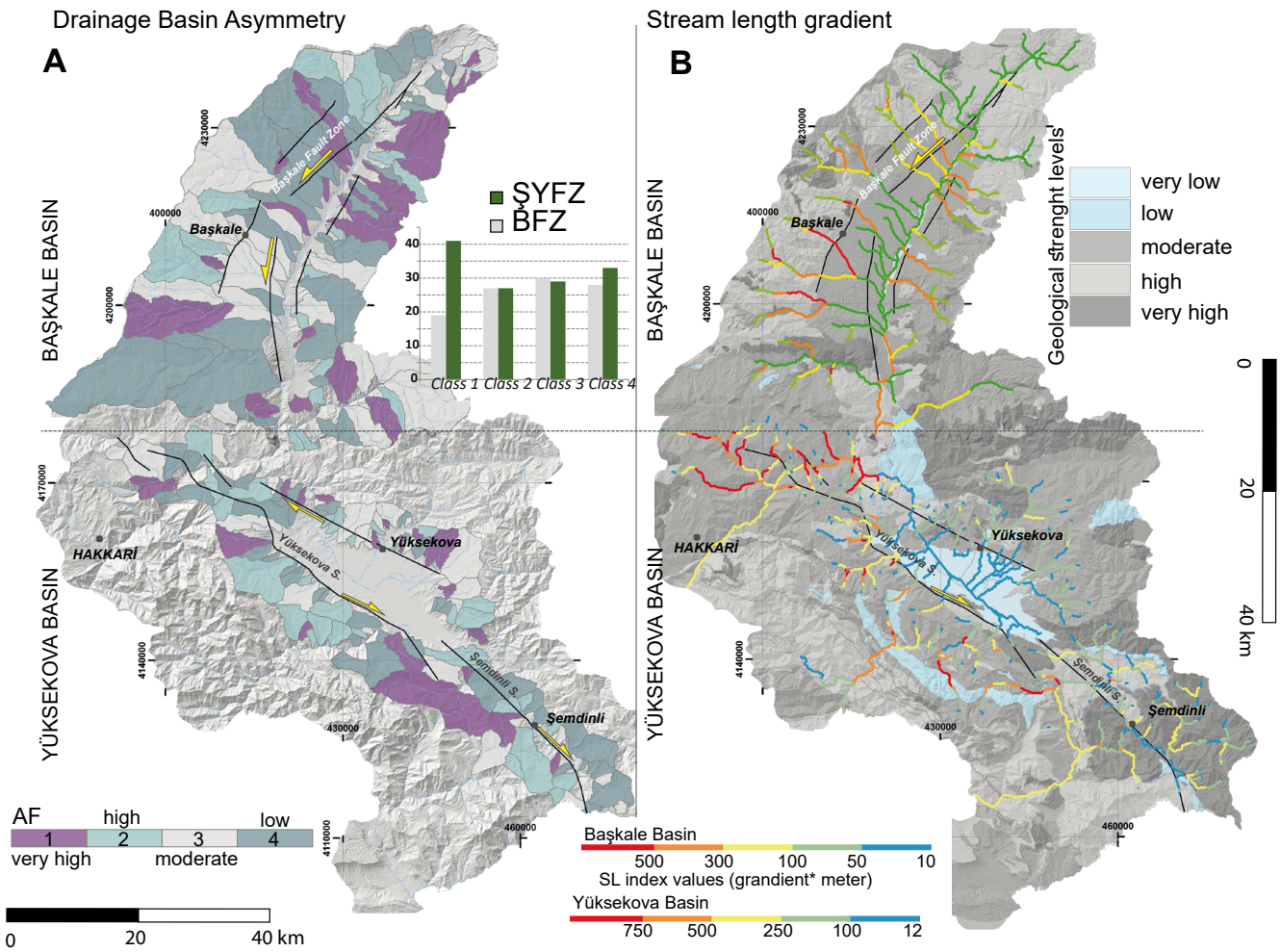

FIGURE 11. Schematic map of the calculated AF and SL indices. A) AF map of the Başkale Basin. The table in the figure shows the distribution of basins under the control of the ŞYFZ and BFZ across classes 1, 2, 3 and 4. The basins with the highest degree of asymmetry, which fall under class 1, are predominantly located within the area controlled by the SYFZ.B) Map of the SL index calculated in the study area.

1.23, with the segments located in the southeastern part of the Yüksekova Basin (S1, S2, S3) exhibiting values closest to 1. These segments represent tectonically highly active and continuously uplifting mountain fronts compared to the others. The steeply inclined mountain fronts and well-defined linear morphology of these segments are also clearly observable in field photographs (Figs. 9B; 12C). The average Smf values measured on the BFZ and the ŞYFZ are 1.14 and 1.11, respectively. Since these two values are close to each other, both the BFZ and the ŞYFZ have been classified within the first tectonic class (Table 1).

Hypsometric integral

HI values were calculated for the sub-basins controlled by both the ŞYFZ and the BFZ, and the calculated data are provided in the Appendix Tables IV and V. Within the Başkale Basin, 33 sub-basins were found with HI values exceeding 0.5, while 61 sub-basins had HI values between 0.3 and 0.5, and 8 sub-basins exhibited HI values below 0.3 (Fig. 13B). Young basins were predominantly observed in the northwestern section of the Başkale fault zone. In the Yüksekova basin, 34 sub-basins exhibited HI values greater than 0.5, while 89 sub-basins had HI values between 0.3 and 0.5. Additionally, 4 sub-basins were identified with HI values less than 0.3 (Fig. 13B). It has been determined that the northern parts of the sub-basins deformed by ŞYFZ exhibit high values. These regions are basins that can also be linked to the BZSZ (Fig. 2). These young basins are located near the bends of the overthrust zone. A comparison of the hypsometric integral values for both fault zones indicates that the Yüksekova Basin comprises younger basins, with higher average values observed in this area. Since the average values of the HI index calculated for the sub-basins controlled by both the ŞYFZ and the BFZ are close to each other, both fault

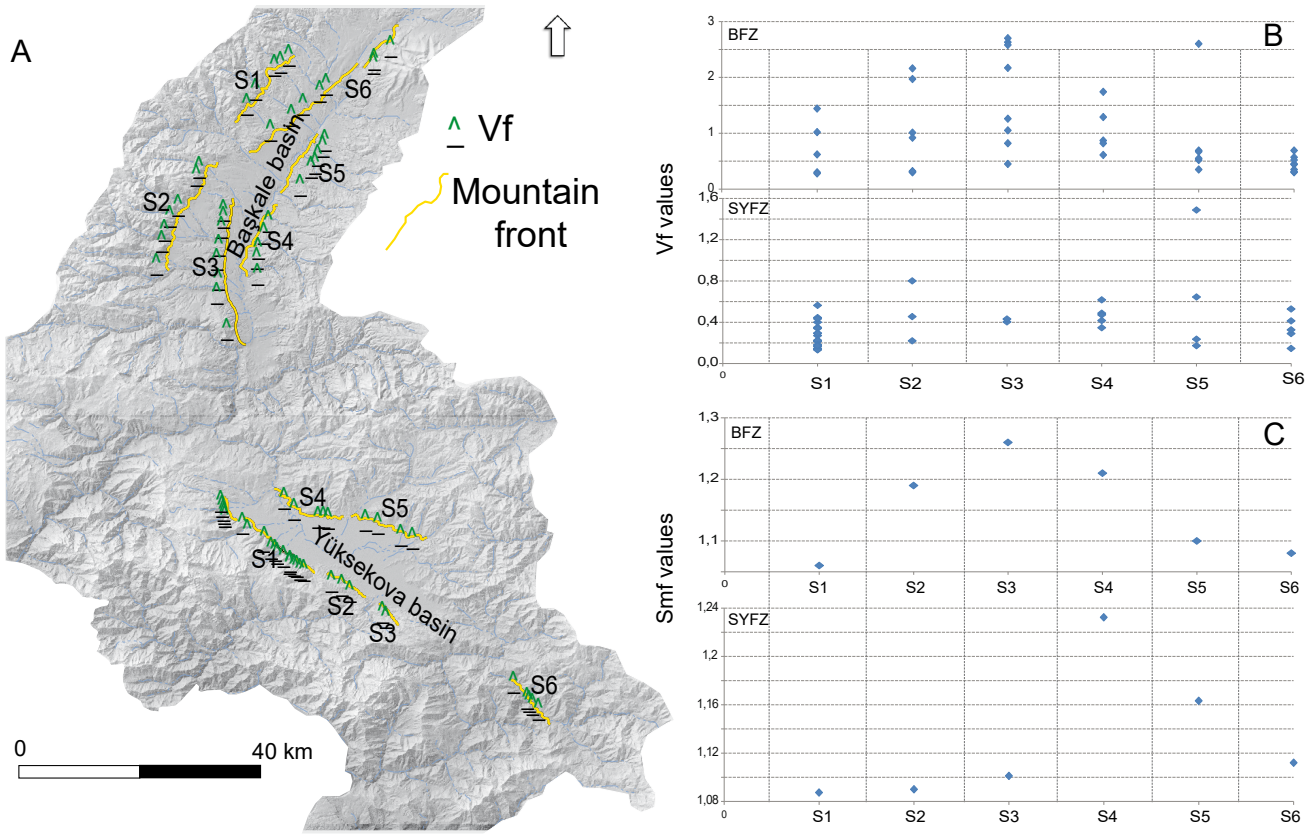

FIGURE 12. A) Schematic watershed map of the study area showing the Smf and Vf location used for the calculation. B) Graph of Vf (Valley Floor Width-to-Height Ratio) values measured along the BFZ and ŞYFZ. C) Graph of Smf (Mountain Front Sinuosity) values measured along the BFZ and ŞYFZ.

zones have been classified within the first tectonic class in terms of the HI index.

Surface roughness

The highest Surface Roughness (SR) value recorded in the Başkale fault zone basin is 2, whereas for the Şemdinli-Yüksekova basin, this value reaches 3.46 (Fig. 13A). Notably, values in the sections of the Şemdinli-Yüksekova fault that are adjacent to the Bitlis Zagros thrust zone rise to as high as 3.5. High SR values were recorded in alignment with the fold axis of the BZSZ on the northern side of the Yüksekova Basin (Fig. 13A). The maximum SR values for the Başkale fault are noted in the northwest section of the Başkale basin. The high SR values (close to 3.5) observed near the BZSZ are attributed to pronounced slope variations and the presence of fold axes formed under the influence of the thrust zone. While the maximum SR value on the BFZ reaches 2.33, it increases up to 3.46 on the ŞYFZ. However, on a basin-scale assessment, the average SR values for both fault zones are approximately 1.07. Therefore, both the BFZ and ŞYFZ are classified as belonging to the second tectonic class in terms of the SR index (Table 1).

Normalized channel steepness index

The results of the Ksn analysis conducted in the study area were classified using an interpolation method, leading to values in a range between 15 and 960 (Fig. 14A; Appendix Table VI). The highest Ksn values in the region are observed in the northwestern part of the Yüksekova Basin, reaching up to approximately 960. In contrast, the Ksn values in the Başkale Basin are around 300, with the highest values particularly concentrated in the western and southwestern parts of the basin (Fig. 14A). The highest Ksn values in the Başkale Basin are located in the eastern and southern parts of the basin. When these high values are compared with the lithological map, it is observed that the high Ksn values in the eastern part correspond to the marble and re-crystallized limestone units, while those in the southern part are associated with the clastic and carbonate rock units (Fig. 14B). However, marble, re-crystallized limestone, and clastic and carbonate rocks are distributed heterogeneously throughout the basin, and low Ksn values have also been measured in other areas where these units are present. Therefore, the influence of lithology on Ksn values has been considered in the basin-scale interpretation. Localized high Ksn values are also observed in the Yüksekova Basin. In particular, the northwestern segment of the ŞYFZ

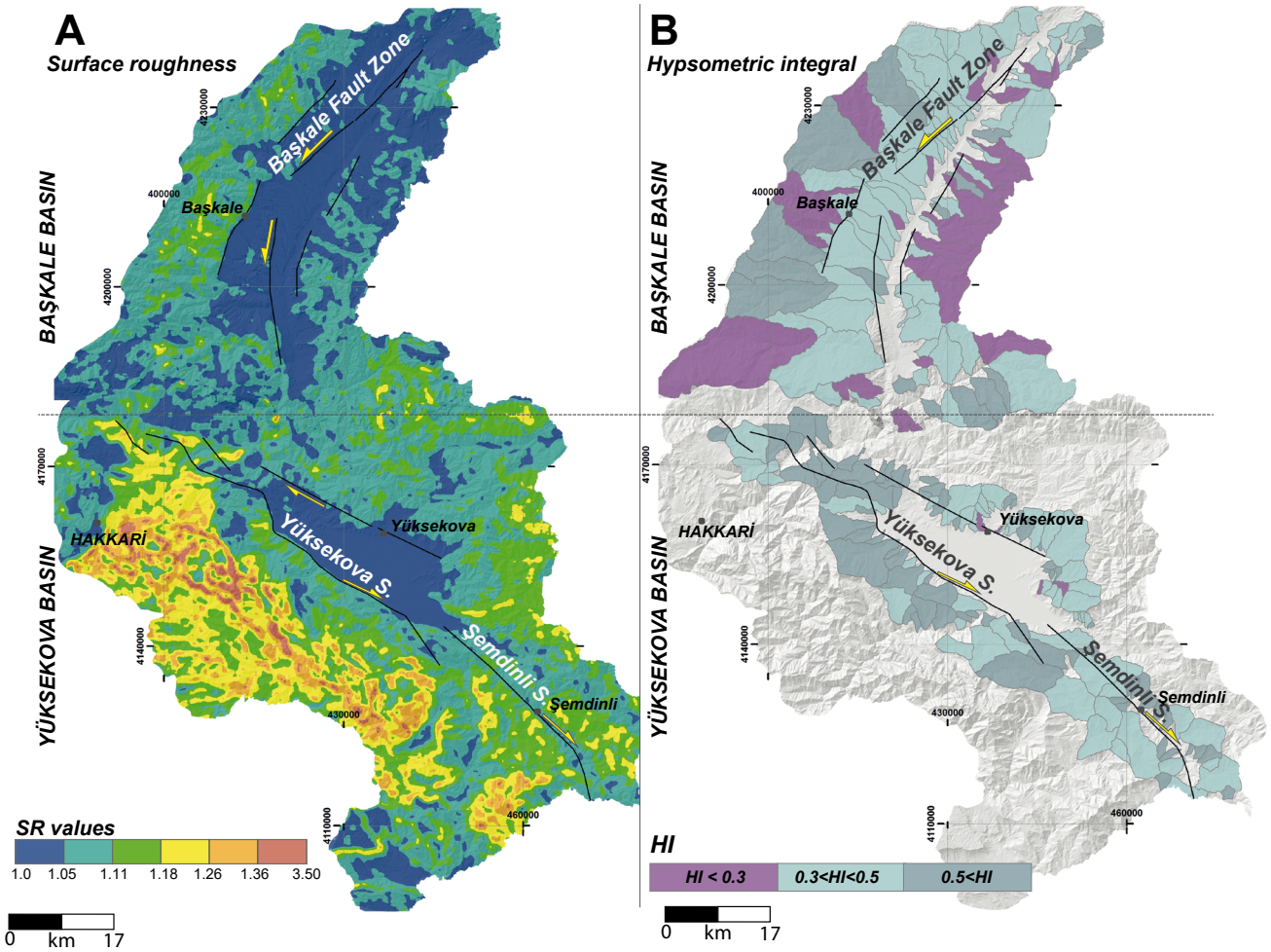

FIGURE 13. Representation of HI and SR values within the study area: A) SR values, B) HI values.

exhibits notably high Ksn values (Fig. 14A). These locations are predominantly composed of clastic and carbonate rock units, representing relatively homogeneous rock groups according to the Selby classification (Fig. 14B). Therefore, the potential strong control of lithology on the Ksn values in this area can be ruled out. The northwestern part of the ŞYFZ stands out as the zone where SL, SR and Ksn indices reach their highest values. Notably, this area also corresponds to the epicenter of the Mw 5.8 earthquake that occurred on January 25, 2005 (Fig. 2B). When the Ksn values of both fault zones are compared, higher values are observed along the ŞYFZ. Based on these values, the BFZ is classified as tectonic class II, whereas the ŞYFZ is categorized as tectonic class I in terms of Ksn index (Table 1).

DISCUSSION

The faults located within the EAPS can be listed from north to south as the Iğdır fault zone, the Doğubayazıt fault, the Balık Gölü fault zone, the Çaldıran fault, the Erciş fault, the Hasantimur fault, the Saray fault zone,and finally, the BFZ and the ŞYFZ, which constitute the focus of this study. These faults form an eastward-convex alignment and continue into the ıranian territory, sharing displacement and deformation among themselves and ultimately transferring deformation toward the North Tabriz fault (Berberian, 1996; Djamour *et al.*, 2011; Mutlu, 2025; Reilinger *et al.*, 2006; Sağlam Selçuk and Kul, 2021). Based on morphometric index analyses conducted along the Iğdır fault zone, located to the Northwest of Mount Ararat, it has been suggested that the southeastern end of the fault reflects relatively higher tectonic activity (Mutlu, 2025). The basins that most clearly reflect this tectonic activity are situated northwest of Mount Ararat (Mutlu, 2025). In the case of the Doğubayazıt fault, the northwestern segment appears to exhibit relatively more pronounced morphotectonic activity (Çakar, 2023; Çakar *et al.*, 2022). Another fault within the shear zone, the Balık Gölü fault zone, displays relatively higher tectonic activity in its northeastern part, based on both morphotectonic

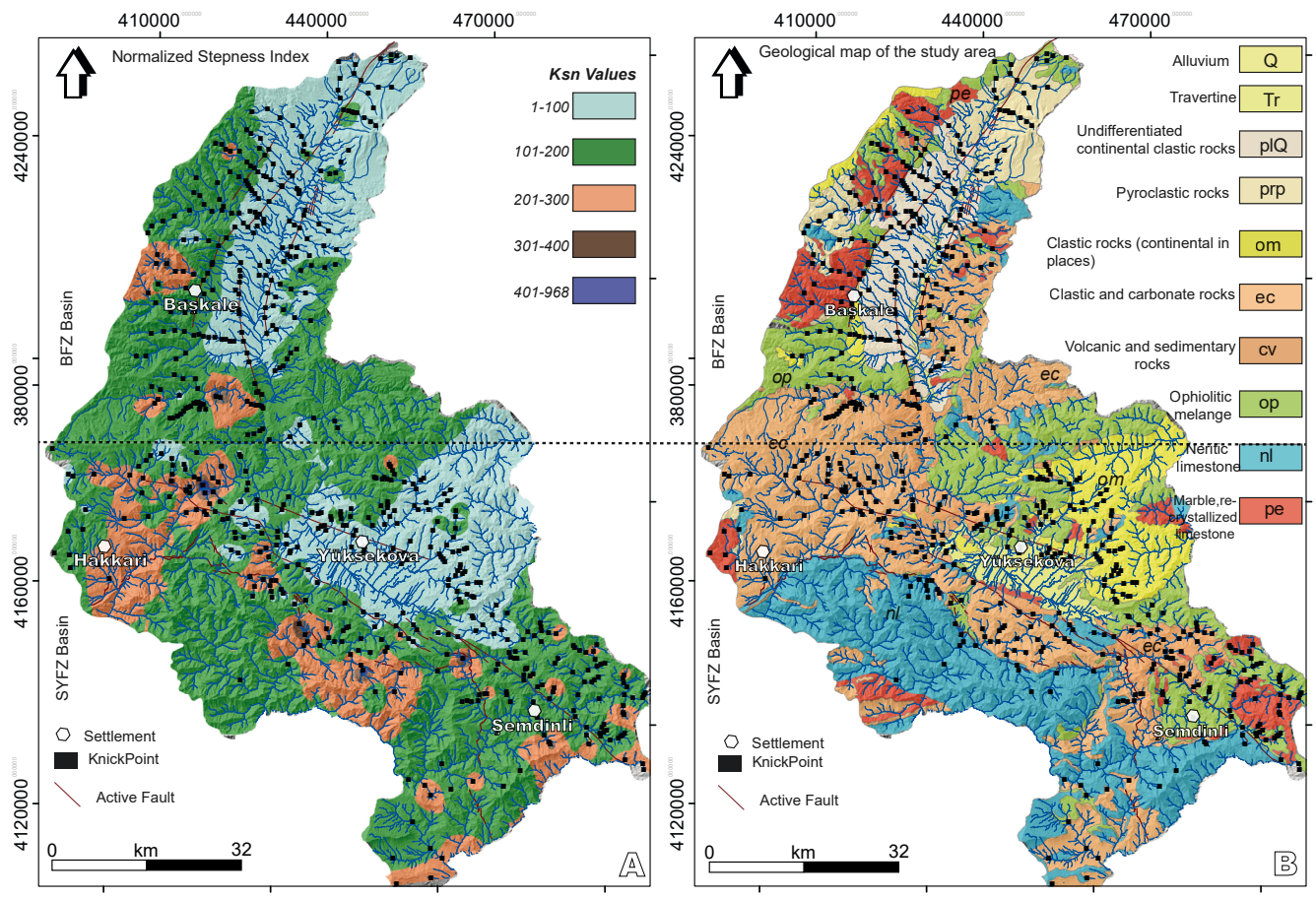

FIGURE 14. A) Sensitivity map of the normalized channel index (Ksn) of the study area to tectonic activity. B) Spatial distribution of Ksn points in the study area in relation to geological units on the map.

indicators and morphometric index results (Mutlu, 2022; Nar, 2023). According to morphometric index results for the Erciş fault, the uplift rates of the northwestern and southeastern segments are relatively higher compared to the central segments (Sağlam Selçuk and Kul, 2021). All of these faults are characterized as right-lateral strike-slip faults. Existing studies have generally assessed these faults individually and on a segment basis. In contrast, this study evaluates the left-lateral strike-slip BFZ and the right-lateral strike-slip ŞYFZ as integrated tectonic systems, each within its own structural context.

All active faults within the EAPS, except for the BFZ, are characterized by right-lateral strike-slip and thrust faulting mechanisms (Figs. 1; 2). This indicates that the deformation within the block is primarily controlled by right-lateral strike-slip faults and thrust faults. According to rigid block models derived from GPS data, the Hakkari Block —which encompasses the Başkale and Yüksekova basins— rotates counterclockwise (Djamour *et al.*, 2011; Reilinger *et al.*, 2006). The morphometric index results obtained in this study also support this tectonic pattern. Quantitative data suggest that the western portions of both the BFZ and the ŞYFZ reflect more intense tectonic activity (Figs. 11; 12; 13; 14).

In terms of morphotectonic indicators, the ŞYFZ presents a greater number and variety of features compared to the BFZ. In particular, the northwestern termination of the ŞYFZ is noteworthy due to its prominent morphological offsets and high morphometric index values (Fig. 8B). Additionally, the fault trace of the ŞYFZ can be followed continuously for approximately 40km, along which well-preserved geomorphic features such as triangular facets and fault scarps represent the most active expressions of fault morphology. Notably, the ŞYFZ has been previously identified as a seismic gap by Demirtaş and Yılmaz (1996), and the lack of both historical and instrumental earthquake records along this fault —when considered together with the morphometric findings of this study— suggests a significant earthquake hazard potential. In contrast, the BFZ is associated with both historical and instrumental

seismicity (AFAD-DDB, 2024; Ambraseys, 2009). Furthermore, the BFZ exhibits fewer morphotectonic indicators and lower morphometric index values compared to the ŞYFZ, implying relatively lower surface tectonic activity.

This study demonstrated that the data obtained from remote sensing and field investigations align well with the results of the morphometric analysis, The sum of morphometric indices analyzed in this work suggests that ŞYFZ accumulates a greater amount of deformation. Morphometric analysis specific to basins and streams have been shown to indicate greater deformation anomalies than the regional averages, particularly in the segments of the Şemdinli-Yüksekova fault zone near the BZSZ. These findings have been validated through field observations. The comparative assessment of morphotectonic indices and geomorphic anomalies indicates that the ŞYFZ exhibits a markedly higher level of neotectonic activity than the BFZ. The presence of a well-developed pull-apart basin (Yüksekova Basin), a sharply defined linear fault trace, and a cumulative stream and ridge offset of 513±56.43m near Yuvalı Village provide robust evidence of sustained lateral displacement along the ŞYFZ. Multiple sequential stream offsets —62±6.8m, 66±7.2m and 95±10.4m— measured near Gürdere Village further support the progressive nature of strike-slip faulting in the central segment of the basin. Geological mapping corroborates a total right-lateral offset of 7.8±0.85km, highlighting the long-term tectonic evolution of the fault. Quantitative morphometric indicators reinforce this interpretation: the ŞYFZ is categorized in the first tectonic class based on SL, Vf, AF and Ksn indices, while the BFZ is consistently ranked in the second or third classes. Although Smf and HI values yield comparable classifications for both zones, higher SR and Ksn values concentrated in the northwestern segment of the ŞYFZ —spatially coinciding with the epicenter of the 2005 Mw 5.8 earthquake— suggest intensified tectonic forcing in that region. These multi-criteria findings collectively underscore the relatively higher tectonic activity and landscape rejuvenation associated with the Şemdinli-Yüksekova fault zone.

CONCLUSION

In this study, seven geomorphic indices were calculated for areas influenced by the ŞYFZ and BFZ, and the obtained data were validated through morphological markers and surface deformation observations (Table 1). A detailed summary of the applied morphometric indices is provided in Table VII. The arithmetic means of the morphometric analyses indicate the dominant active tectonic regime in the region. Both fault zones exhibit young topographic features and morphotectonic indicators confirming ongoing active deformation. By classifying the geomorphic index values, regional tectonic activity levels were assessed, with pronounced anomalies particularly detected in the northwestern part of the ŞYFZ. IAT value derived from the analyses quantitatively reflects the rate of deformation. In the IAT classification, the BFZ falls within the moderate tectonic class, whereas the ŞYFZ is categorized within the high tectonic class. Considering the clearly observable geomorphological traces and elevated morphometric activity values of the ŞYFZ together, it is inferred that this fault has not released its accumulated strain in the recent geological past and should therefore be regarded as a seismic gap. Consequently, the ŞYFZ poses a significant earthquake hazard potential.

ACKNOWLEDGMENTS

The author expresses gratitude to Azad Saglam Selcuk and Ahmet Ozkan Kul for their assistance in preparing the Figures. The author sincerely acknowledges Maria Ortuño Candela for her insightful comments and constructive suggestions, which greatly contributed to the enhancement of this manuscript. Additionally, he extends his thanks to the editor and referees of Geologica Acta for their valuable comments and suggestions.

REFERENCES

AFAD-DDB (Republic of Türkiye, Ministry of Interior, Disaster and Emergency Management Authority – Earthquake Department Presidency), 2024. Earthquake Data. Ankara, Disaster and Emergency Management Authority, Earthquake Department, Last accessed: March 10, 2024. Website: https://deprem.afad.gov.tr/ddakatalogu

Akkaya, İ., 2015. The Application of HVSR microtremor survey method in Yüksekova (Hakkari) region, Eastern Turkey. Journal of African Earth Sciences, 109, 87-95.

Ambraseys, N., 2009. Earthquakes in the Mediterranean and Middle East: a multidisciplinary study of seismicity up to 1900. Cambridge, Cambridge University Press, 946pp.

Ambraseys, N.N., Finkel, A.C., 1995. The seismicity of Turkey and adjacent areas: A historical review, 1500-1800. Istanbul, M.S. Eren Beyoğlu, 240pp.

Andreani, L., Gloaguen, R.J.E.S.D., 2016. Geomorphic analysis of transient landscapes in the Sierra Madre de Chiapas and Maya Mountains (northern Central America): implications for the North American–Caribbean–Cocos plate boundary. Earth Surface Dynamics, 4(1), 71-102.

Andreani, L., Stanek, K.P., Gloaguen, R., Krentz, O., Domínguez-González, L., 2014. DEM-based analysis of interactions between tectonics and landscapes in the Ore Mountains and Eger Rift (East Germany and NW Czech Republic). Remote Sensing, 6(9), 7971-8001.

Atalay, K., 2007. January 25, 2005 Hakkari earthquake source properties and seismotectonic characteristics. Master's Thesis. YYU Institute of Science and Technology, 45pp.

Berberian, M., 1981. Tectono-Plutonic Episodes in Iran. In: Gupta, H.K., Delany, F.M. (eds.). Zagros, Hindu Kush, Himalaya: Geodynamic Evolution, Geodynamics Series 3. American Geophysical Union, 5-32.

Berberian, M., 1996. The historical record of earthquakes in Persia, Encyclopaedia Iranica. Costa Mesa (California), Mazda Publishers, vol. VII, 635-640.

Bishop, P., Hoey, T.B., Jansen, J.D., Artza, I.L., 2005. Knickpoint recession rate and catchment area: the case of uplifted rivers in Eastern Scotland. Earth Surface Processes and Landforms, 30(6), 767-778.

Blum, M.D., Törnqvist, T.E., 2000. Fluvial responses to climate and sea-level change: a review and look forward. Sedimentology, 47, 2-48.

Boray, A., 1975. Structure and metamorphism of the Bitlis region. Geology Bulletin of Turkey, 18, 81-84.

Bull, W.B., 1977. Tectonic geomorphology of the Mojaand Desert, California, U.S. Geological Surandy Contract Report, 14-0-001-G-394.

Bull, W.B., 2007. Tectonic Geomorphology of Mountains: A New Approach to Paleoseismology. USA, Wiley Blackwell, 316pp.

Bull,W.B., Mcfadden, L.M., 1977 Tectonic geomorphology north and south of the Garlock Fault, California. Jour. Geomorphology, 1, 15-32.

Burbank, D.W., Anderson, R.S., 2013. Tectonic Geomorphology. Oxford, Blackwell Science, 2nd edition, 287pp.

Chang, L., Flesch, L.M., Wang, C.Y., Ding, Z., 2015. Vertical coherence of deformation in lithosphere in the eastern Himalayan syntaxis using GPS, Quaternary fault slip rates, and shear wave splitting data. Geophysical Research Letters, 42(14), 5813-5819.

Cheng, F., Jolivet, M., Fu, S., Zhang, C., Zhang, Q., Guo, Z., 2016. Large-scale displacement along the Altyn Tagh Fault (North Tibet) since its Eocene initiation: Insight from detrital zircon U–Pb geochronology and subsurface data. Tectonophysics, 677, 261-279.

Çakar, S., 2023. Segmentation and tectonic geomorphology of the Doğubayazit fault (Agrı). Master's Thesis. Van (Turkey). Van Yüzüncü Yıl University, 107pp.

Çakar, S., Kul, A.Ö., Mutlu, S., Çiftçi Nar, A., Sağlam Selçuk, A., 2022. Identification of Tectono-Geomorphological Structures Developed Along the Doğubayazıt Fault Using Morphometric Analyses. Ankara, 74th Geological Congress of Turkey with International Participation, 15pp.

Day, M.J., 1979. Surface roughness as a discriminator of tropical karst styles in problems in karst environments. Zeitschrift für Geomorphologie, 32 (Supplementband Stuttgart), 1-8.

Dehbozorgi, M., Pourkermani, M., Arian, M., Matkan, A.A., Motamedi, H., Hosseiniasl, A., 2010. Quantitative analysis of relative tectonic activity in the Sarvestan area, central Zagros, Iran. Geomorphology, 121(3-4), 329-341.

Demirtaş, R. Yilmaz, R., 1996. Seismotectonics of Turkey. Ministry of Public Works and Settlement, General Directorate of Disaster Affairs, Earthquake Research. Department, Ankara, 35pp.

Dewey, J.F., Hempton, M.R., Kidd, W.S.F., Saroglu, F.A.M.C., Şengör, A.M.C., 1986. Shortening of continental lithosphere: the neotectonics of Eastern Anatolia—a young collision zone. London, The Geological Society, 19(1, Special Publications), 1-36.

DiBiase, R.A., Whipple, K.X., Heimsath, A.M., Ouimet, W.B., 2010. Landscape form and millennial erosion rates in the San Gabriel Mountains, California. Earth and Planetary Science Letters, 289(1-2), 134-144. DOI: https://doi.org/10.1016/j.epsl.2009.10.036

Djamour, Y., Bayer, R., Tavakkoli, F., Vernant, P., 2003. GPS network monitoring the tectonic deformation on the Tehran area (Iran) between 2000 and 2002. European Geophysical Society–American Geophysical Union–European Union of Geosciences (EGS-AGU-EUG) Joint Assembly, 6503pp.

Djamour, Y., Andrnant, P., Nankali, H.R., Tavakoli, F., 2011. NW Iran-eastern Turkey present-day kinematics: Results from the Iranian permanent GPS network. Earth and Planetary Science Letters, 307, 27-34. DOI: 10.1016/j.epsl.2011.04.029

El Hamdouni, R., Irigaray, C., Fernández, T., Chacón, J., Keller, E.A., 2008. Assessment of relative active tectonics, southwest border of the Sierra Nevada (southern Spain). Geomorphology, 96(1-2), 150-173. DOI: https://doi.org/10.1016/j.geomorph.2007.08.004

Emre, Ö., Doğan, A., Özalp, Ö., Yıldırım, Y., 2005. 25 Ocak 2005 Hakkari Depremi Hakkında Ön Değerlendirme. Ankara (Turkey), General Directorate of Mineral Research & Exploration (MTA), Report No. 123, 5pp.

Emre, Ö., Duman, T.Y., Özalp, S., Olgun, Ş., Elmacı, H., 2012. 1:250,000 Scale Active Fault Map Series of Turkey, Ağrı (NJ 38-1) Sheet. Ankara (Turkey), General Directorate of Mineral Research and Exploration (MTA) Publications, 24pp.

Emre, Ö., Duman, T., Özalp, S., Elmacı, H., Olgun, Ş., Şaroğlu, F., 2013. Active Fault Map of Turkey with an Explanatory Text. 1:1,250,000 Scale. Ankara (Turkey), General Directorate of Mineral Research and Exploration (MTA), Special Publication Series 30. ISBN: 978-605-5310-56-1

Ergin, K., Güçlü, U., Uz, Z., 1967. A Catalogue of earthquakes for Turkey and surrounding area (11 A.D. to 1964 A.D.). Istanbul (Turkey), Istanbul Technical University (ITU), Faculty of Mines, Institute of Physics of the Earth, Technical Report No. 24, 216pp.

Esmaeil, H., Solgi, A., Pourkermani, M., Matkan, A., Mehran, A., 2017. Assessment of relative active tectonics in the Bozgoush Basin (SW of Caspian Sea). Open Journal of Marine Science, 7, 211-237.

Ferrari, J.A., Hiruma, S.T., Karmann, I., 1998. Caracterização morfométrica de uma superfície cárstica do Vale do Ribeira, São Paulo (Núcleo Caboclos- PETAR). Revista do Instituto Geológico, 19, 9-17.

Ferrater, M., Booth-Rea, G., Pérez-Peña, J.V., Azañón, J.M., Giaconia, F., Masana, E., 2015. From extension to

transpression: quaternary reorganization of an extensional related drainage network by the Alhama de Murcia strike-slip fault (eastern Betics). Tectonophysics, 663, 33-47.

Flint, J.J., 1974. Stream gradient as a function of order, magnitude, and discharge. Water Resources Research, 10, 969-973.

Font, M., Amorese, D., Lagarde, J.L., 2010. DEM and GIS analysis of the stream gradient index to evaluate effects of tectonics: the Normandy intraplate area (NW France). Geomorphology, 119(3-4), 172-180. DOI: https://doi.org/10.1016/j.geomorph.2010.03.017

Giaconia, F., Booth-Rea, G., Martínez-Martínez, J.M., Azañón, J.M., Pérez-Peña, J.V., 2012. Geomorphic analysis of the Sierra Cabrera, an actiand pop-up in the constrictional domain of conjugate strike slip faults: The Palomares and Polopos fault zones (eastern Betics, SE Spain). Tectonophysics, 580, 27-42. DOI: 10.1016/j.tecto.2012.08.028

Gold, R.D., Cowgill, E., Arrowsmith, J.R., Gosse, J., Chen, X., Wang, X.F., 2009. Riser diachroneity, lateral erosion, and uncertainty in rates of strike-slip faulting: A case study from Tuzidun along the Altyn Tagh Fault, NW China. Journal of Geophysical Research, Solid Earth, 114(B4), 1-24.

Gold, R.D., Cowgill, E., Arrowsmith, J.R., Chen, X., Sharp, W.D., Cooper, K.M., Wang, X.F., 2011. Faulted terrace risers place new constraints on the late Quaternary slip rate for the central Altyn Tagh fault, northwest Tibet. Geological Society of America Bulletin, 123(5-6), 958-978.

GRASS (Geographic Resources Analysis Support System) Development Team, 2009. Geographic Resources Analysis Support System (GRASS GIS) Software, version 6.3.0. Last accessed: Website: http://www.grass. osgeo.org

Grohmann, C.H., 2004a. Morphometric analysis in Geographic Information Systems: applications of free software GRASS and R. Computers & Geosciences, 30(9-10), 1055-1067. DOI: https://doi. org/10.1016/j.cageo.2004.08.002

Grohmann, C.H., 2004b. Tecnicas de geoprocessamento aplicadas a analise morfometrica. M.Sc. Thesis. Sao Paulo, Universidade de Sao Paulo, Instituto de Geociencias, 78pp.

Grohmann, C.H., Riccomini, C., 2009. Comparison of roving-window and search-window techniques for characterising landscape morphometry. Computers & Geosciences, 35(10), 2164-2169. DOI: https://doi.org/10.1016/j.cageo.2008.12.014

Grohmann, C.H., Riccomini, C., Alves, F.M., 2007. SRTM-based morphotectonic analysis of the Poços de Caldas Alkaline Massif, southeastern Brazil. Computers & Geosciences, 33(1), 10-19.

Göncüoğlu, M.C., Turhan, N., 1984. Geology of the Bitlis metamorphic belt. In Geology of the Taurus belt. International Symposium on the Geology of the Taurus Belt Maden Tetkik ve Arama Genel Müdürlüğü yayınları. In: Tekeli, O., ve Göncüoğlu, M.C. (eds.). 237-244.

Hack, J.T., 1957. Studies of longitudinal profiles in Virginia and Maryland. Washington, U.S. Geological Survey, United States Government Printing Office, Professional Paper 294-B, 1.

Hack, J.T., 1973. Stream-profile analysis and stream-gradient index. Journal of Research of the U.S. Geological Survey, 1(4), 421-429. Website: https://pubs.usgs.gov/journal/1973/vol1/issue4/

Hakanson, L., 1974. A mathematical model for establishing numerical values of topographical roughness for lake bottoms. Geografiska Annaler, Series A, Physical Geography, 56, 183-200.

Hare, P.W., Gardner, T.W., 1985. Geomorphic indicators of vertical neotectonismtectonics along converging plate margins, Nicoya Peninsula, Costa Rica. Tectonic geomorphology, 4, 75-104.

Hessami, K., Pantosti, D., Tabassi, H., Shabanian, E., Abbassi, M.R., Feghhi, K., Solaymani, S., 2003. Paleoearthquakes and slip rates of the North Tabriz Fault, NW Iran: preliminary results. Annals of Geophysics, 46(5), 14pp.

Hilley, G.E., Arrowsmith, J.R., 2008. Geomorphic response to uplift along the Dragon's Back pressure ridge, Carrizo Plain, California. Geology, 36(5), 367-370. DOI: https://doi.org/10.1130/G24662A.1

Hobson, R.D., 1972. Surface roughness in topography: quantitative approach. In: Chorley, R.J. (ed.). Spatial analysis in geomorphology. Routledge, 225-245.

Hull, A., Augello, A., Erdik, M., Turfan, M., Pavone, M., Atay, E., 2002. Seismic hazard assessment for the Hakkari project. International Journal on Hydropower & Dams, 9(5), 66-70.

Karakhanian, A.S., Trifonov, V.G., Philip, H., Avagyan, A., Hessami, K., Jamali, F., Bayraktutan, M.S., Bagdassarian, H., Arakelian, S., Davtian, V., Adilkhanyan, A., 2004. Active faulting and natural hazards in Armenia, eastern Turkey and northwestern Iran. Tectonophysics, 380, 189-219.

Karmann, I., Pereira, R.F., Ferrari, J.A, 1996. Índice de ru gosidade: parâmetro morfométrico da intensidade de relevo. Exemplo do carste da bacia do Rio Una, Bahia. Anais, 4, 575-579.

Keller, E.A., ve Pinter, N., 2002. Active Tectonics: Earthquakes, Uplift, and Landscape. New Jersey, Prentice Hall, 362pp.

Khalifa, A., Cakir, Z., Owen, L., Kaya, Ş., 2018. Morphotectonic analysis of the east Anatolian fault, Turkey. Turkish Journal of Earth Sciences, 27(2), 110-126.

Kirby, E., Whipple, K.X., 2012. Expression of active tectonics in erosional landscapes. Journal of structural geology, 44, 54-75.

Koçyiğit, A., 2005. Origin of the Sutluce (Hakkari) Earthquake: Baskale Fault Zone, SE Turkey). Earthquake Symposium, Denizli, Turkey.

Koçyiğit, A., Yilmaz, A., Adamia, S., Kuloshvili, S., 2001. Neotectonics of East Anatolian Plateau (Turkey) and Lesser Caucasus: implication for transition from thrusting to strike-slip faulting. Geodinamica Acta, 14(1-3), 177-195.

Kumar, N., Dumka, R.K., Mohan, K., Chopra, S., 2022. Relative active tectonics evaluation using geomorphic and drainage indices, in Dadra and Nagar Haveli, western India. Geodesy and Geodynamics, 13(3), 219-229.

Lamb, M.P., Fonstad, M.A., 2010. Rapid formation of a modern bedrock canyon by a single flood event. Nature Geoscience, 3(7), 477-481. DOI: https://doi.org/10.1038/ngeo894

Lavé, J., Avouac, J.P., 2001. Fluvial incision and tectonic uplift across the Himalayas of central Nepal. Journal of Geophysical Research: Solid Earth, 106(B11), 26561-26591.

Mckenzie, D., 1970. Plate tectonics of the Mediterranean region. Nature, 226(5242), 239-243.

McKenzie, D., 1972. Active tectonics of the Mediterranean region. Geophysical Journal International, 30(2), 109-185.

Mutlu, S., 2022. Paleosismological features and segmentation of the lake Balık fault zone (Doctoral dissertation). Van (Turkey), Van Yüzüncü Yıl University, 217pp.

Mutlu, S., 2025. The Significance and Morphotectonic Features of the Iğdır Fault within the Eastern Anatolian Compressional Tectonic Block. Geological Bulletin of Turkey, 68(2), 225-258.

Nar, A., 2023. Internal deformation evolution of East Anatolian Tectonic Block: Determining the morphotectonic properties and long term slip rate of Balik Lake Fault Zone (Ağri). (Doctoral dissertation). Van (Turkey), Van Yüzüncü Yıl University, 253pp.

Ouimet, W.B., Whipple, K.X., Granger, D.E., 2009. Beyond threshold hillslopes: Channel adjustment to base-level fall in tectonically active mountain ranges. Geology, 37(7), 579-582.

Özsayın, E., 2016. Relative tectonic activity assessment of the Çameli Basin, Western Anatolia, using geomorphic indices. Geodinamica Acta, 28(4), 241-253.

Özsayin, E., Dirik, K., Ocakoğlu, F, Açikalin Cartigny, S., Sağlam Selçuk, A., 2023. Tectonic Geomorphology of Bozdoğan and Karacasu Grabens, Western Anatolia. Geologica Acta, 21.1, 1-14.

Philip, H., Avagyan, A., Karakhanian, A., Ritz, J.F., Rebai, S., 2001. Estimating slip rates and recurrence intervals for strong earthquakes along an intracontinental fault: example of the Pambak–Sevan–Sunik fault (Armenia). Tectonophysics, 343(3-4), 205-232.

Pike, R.J., Wilson, S.E., 1971. Elevation-relief ratio, hypsometric integral, and geomorphic area-altitude analysis. Geological Society of America Bulletin, 82(4), 1079-1084.

Pánek, T., 2004. The use of morphometric parameters in tectonic geomorphology (of the example of the Western Beskidy Mts). Acta Universitatis Carolinae, Geographica, 1, 111-126.

Pérez-Peña, J.V., Azañón, J.M., Azor, A., 2009a. CalHypso: An ArcGIS extension to calculate hypsometric curves and their statistical moments. Applications to drainage basin analysis in SE Spain. Computers & Geosciences, 35(6), 1214-1223.

Pérez-Peña, J.V., Azañón, J.M., Booth-Rea, G., Azor, A., Delgado, J., 2009b. Differentiating geology and tectonics using a spatial autocorrelation technique for the hypsometric integral. Journal of Geophysical Research: Earth Surface, 114(F2), 1-15.

Pérez-Peña, J.V., Azor, A., Azañón, J.M., Keller, E.A., 2010. Actiand tectonics in the Sierra Nevada (Betic Cordillera, SE Spain): Insights from geomorphic indexes and drainage pattern analysis. Geomorphology, 119, 74-87. DOI: DOI: 10.1029/2008JF001092

Reilinger, R., McClusky, S., Andrnant, P., Lawrence, S., Ergintav, S., Cakmak, R., Ozener, H., Kadirov, F., Guliev, I., Stepanyan, R., 2006. GPS constraints on continental deformation in the Africa-Arabia Eurasia continental collision zone and implications for the dynamics of plate interactions. Journal of Geophysical Research: Solid Earth (1978–2012), 111, 1-26. DOI: 10.1029/2005JB004051

Ricou, L.E., 1971. Le croissant ophiolitique péri-arabe: Une ceinture de nappes mises en place au Crétacé supérieur. Revue de Géographie Physique et de Géologie Dynamique, Deuxième série, 13(4), 327-350.

Rockwell, T.K., Keller, E.A., Johnson, D.L., 1985. Tectonic geomorphology of alluvial fans and mountain fronts near Ventura, California. In: Morisawa, M., Hack, J.T. (eds.). Proceedings of the 15th Annual Geomorphology Symposium, Tectonic Geomorphology. Boston (USA), September 1984, 15th Annual Binghamton Geomorphology Symposium, Allen and Unwin Publishers, 183-207.

Sançar, T., 2018. Investigation of the Uplift Velocity History of the Yüksekova Basin (Southeastern Turkey). Geological Bulletin of Turkey, 61(2), 207-240.

Sançar, T., 2021. Morphometric investigations on the NW Bitlis-Zagros mountain range (SE Turkey): Implications for the internal deformation of the western Turkish-Iranian Plateau. Journal of Asian Earth Sciences, 216, 104751.

Sağlam Selçuk, A., Kul, A., Ö., 2021. Long-term slip rate estimation for Ercis, Fault in East Anatolian Compressive Tectonic Block from geologic and geomorphologic field evidence. Geological Journal, 56(10), 5290-5310. DOI: https:// doi.org/10.1002/gj.4237

Selby, M.J., 1980. A rock strength classification for geomorphic purposes: with tests from Antarctica and New Zealand. Zeitschrift für Geomorphologie, 24, 31-51.

Selçuk, A.S., 2016. Evaluation of the relative tectonic activity in the eastern Lake Van basin, East Turkey. Geomorphology, 270, 9-21.

Selçuk, A.S., Düzgün, M., 2017. Tectonic geomorphology of Başkale Fault zone. Bulletin of the Mineral Research and Exploration, 155(155), 33-46.

Sengör, A.M.C., 1979. The North Anatolian transform fault: its age, offset and tectonic significance. Journal of the Geological Society, 136(3), 269-282.

Seyitoğlu, G., Esat, K., Kaypak, B., Toori, M., Aktuğ, B., 2018. Internal deformation of the Turkish Iranian Plateau in the hinterland of Bitlis-Zagros Suture Zone. In: Farzipour Saein, A. (ed.). Tectonic and Structural Framework of the Zagros Fold Thrust Belt. Elsevier, 161-244.

Shahzad, F., Gloaguen, R., 2011a. TecDEM: A MATLAB based toolbox for tectonic geomorphology, Part 1: Drainage network preprocessing and stream profile analysis. Computers & Geosciences, 37(2), 250-260.

Shahzad, F., Gloaguen, R., 2011b. TecDEM: A MATLAB based toolbox for tectonic geomorphology, Part 2: Surface dynamics and basin analysis. Computers & geosciences, 37(2), 261-271.

Silva, P.G., Goy, J.L., Zazo, C., Bardají, T., 2003. Faulth generated mountain fronts in southeast Spain: Geomorphologic assessment of tectonic and seismic activity. Geomorphology 50, 203-225. DOI: 10.1016/S0169-555X(02)00215-5

Snyder, N.P., Whipple, K.X., Tucker, G.E., Merritts, D.J., 2003. Channel response to tectonic forcing: field analysis of stream morphology and hydrology in the Mendocino triple junction region, northern California. Geomorphology, 53, 97-127.

Soysal, H., Sipahioğlu, S., Koçak, D., Altinok, Y., 1981. Historical Earthquake Catalog of Turkey and Surroundings (2100-MS 1900 BC). Ankara, TUBITAK Project (TBAG).

Steiner, S.S., Machado, R., Grohmann, C.H., 2006. Análise morfométrica da estrutura divergente na região do Rio Paraíba do Sul, Rio de Janeiro. XLIII Congresso Brasileiro de Geologia, Aracaju-SE Anais, 97pp.

Strahler, A.N., 1952. Hypsometric (area-altitude) analysis of erosionincisional topography. Geological society of America bulletin, 63(11), 1117-1142.

Şaroğlu, F., 1985. Geological and Structural Evolution of Eastern Anatolia in the Neotectonic Period. Doctoral dissertation. Istanbul (Turkey), Istanbul University, Science Institute of Sciences, unpublished, 240pp.

Şaroğlu, F., Emre, Ö., Boray, A., 1987. Türkiye'nin diri fayları ve depremsellikleri. General Directorate of Mineral Research & Exploration (MTA), Report No. 394. Rap, 394.

Şaroğlu, F., Emre, Ö, Kuşçu, I., 1992. Turkey Active Fault Map of Turkey) scale 1:2000000. Ankara, General Directorate of Mineral Research and Exploration.

Şenel, M., 2002. 1:100.000 Scale Geology of Turkey Maps No:43 Hakkari-N52 and N53 Plots. Ankara, Mineral Research and Exploration Institute, Geological Surveys Department.

Şenel, M., 2007. 1:100.000 Scale Geology of Turkey Maps No:43 Hakkari-M52 and M53 Plots. Ankara, Mineral Research and Exploration Institute, Geological Survey Department.

Şengör, A.M.C., Yilmaz, Y., 1981. Tethyan evolution of Turkey: a plate tectonic approach. Tectonophysics, 75(3-4), 181-241.

Şengör, A.C., Yazıcı, M., 2020. The aetiology of the neotectonic evolution of Turkey. Mediterranean Geoscience Reviews, 2, 327-339.

Tan, O., Tapırdamaz, M.C., Yörük, A., 2008. The earthquake catalogues for Turkey. Turkish Journal of Earth Sciences, 17(2), 405-418.

Tchalenko, J.S., Braud, J., 1974. Seismicity and structure of the Zagros (Iran): the Main Recent Fault between 33 and 35 N. Philosophical Transactions of the Royal Society of London, Series A, Mathematical and Physical Sciences, 277(1262), 1-25.

Toksöz, M.N., Reilenger, R., 1992. The İnterpretation of Crustal Dynamics Data ın Terms Of Plate Interactıons and Actıve Tectonıcs of the "Anatolian Plate" and Surrounding Regions in the Middle East. Nasa Grant Nag, Final Report, 5-753.

TSMS, 2025. Climate Data. Ankara, Turkish State Meteorological Service. Last accessed: May 2025. Website: https://www.mgm.gov.tr

Whipple, K.X., Tucker, G.E., 1999. Dynamics of the stream-power river incision model: Implications for height limits of mountain ranges. Journal of Geophysical Research: Solid Earth, 104(B8), 17661-17674. DOI: https://doi.org/10.1029/1999JB900120

Whipple, K.X., DiBiase, R.A., Crosby, B.T., 2013. Bedrocks rivers. In: Shroder, J.F. (ed.). Treatise on Geomorphology. Poland, Elsevier, 550-573.

Whittaker, A.C., 2012. How do landscapes record tectonics and climate? Lithosphere, 4(2), 160-164.

Willgoose, G., 1994. A statistic for testing the elevation characteristics of landscape simulation models. Journal of Geophysical Research, 99, 13987-13996. DOI: 10.1029/94JB00123

Wobus, C., Whipple, K.X., Kirby, E., Snyder, N., Johnson, J., Spyropolou, K., Crosby, B., Sheehan, D., 2006. Tectonics from topography: Procedures, promise, and pitfalls. In: Willett, S.D., Hovius, N., Brandon, M.T., Fisher, D.M. (eds.). Tectonics, Climate, and Landscape Evolution. Geological Society of America, 398 (Special Paper), 55-74.

Yılmaz, Y., 1971. Etüde petrographicque et geochronologique de la region de Casa (Partie Meridionale du Masif de Bitlis, Turquie, These de doct 3 cycle). Univ. Sci.Med. Greonable, 230pp.

Yilmaz, O., 1975. The rocks of the Cacas Region (Bitlis Massif) petrographic and stratigraphic investigations. Turkey Geology Bulletin, 18(1), 33-40.

Zebari, M., Grützner, C., Navabpour, P., Ustaszewski, K., 2019. Relative timing of uplift along the Zagros Mountain Front Flexure (Kurdistan Region of Iraq): Constrained by geomorphic indices and landscape evolution modeling. Solid Earth, 10(3), 663-682.

Zygouri, V., Koukouvelas, I.K., Kokkalas, S., Xypolias, P., Papadopoulos, G.A., 2015. The Nisi Fault as a key structure for understanding the active deformation of the NW Peloponnese, Greece. Geomorphology, 237, 142-156.

Manuscript received October 2024;
revision accepted July 2025;
published Online November 2025.